Some Recent Advances in Liquefied Natural Gas (LNG) Production, Spill, Dispersion, and Safety

Walter Chukwunonso Ikealumba and Hongwei Wu*

School of Chemical and Petroleum Engineering, Curtin University, GPO Box U1987, Perth, Western Australia 6845, Australia

ABSTRACT: The global demand of liquefied natural gas (LNG) has risen rapidly in recent years for the reasons of energy security and sustainable development. This has led to considerable recent research interests and efforts in the LNG production chain and associated risks in handling, storage, and transport of LNG, largely driven by the intrinsic process safety issues of LNG, potential terrorist threats, and public confidence in LNG safety. This review presents an overview on some recent advances in the LNG value chain, covering upstream gas production and gathering, liquefaction, shipping, and regasification processes. Recent developments in the experimentation and modeling of LNG spills associated with the LNG value chain are then summarized, covering the events following a LNG spill, including LNG pool formation, vapor dispersion, and combustion. The consequent hazards and safety issues are also discussed, with a focus on the methods for improving the safety of personnel, facilities, and ships. The key technical gaps in the related research areas have been identified, and future research directions are outlined.

1. INTRODUCTION

**1.1. Global Energy Outlook and the Role of Natural Gas.** Global energy demand is rapidly rising at a time when the world needs to respond to the threat of climate change by reducing carbon dioxide emissions, many of which came from the use of fossil fuels. On the basis of BP statistical review of world energy 2013,[1] Figure 1 illustrates the growth of the world energy mix with a forecast to 2030. It clearly depicts the growth in energy consumption by fuel source, with the energy consumption by natural gas approaching that of coal and oil. For the year 2012, with a total energy use of 521.97 EJ [494.73 quadrillion British thermal units (Btu)], oil is the leading source of energy in the world at 33%, closely followed by coal at 30%, natural gas at 24%, nuclear at 4%, and other sources (wind, solar, etc.) at 9%. However, in Australia, the total energy use is 5.26 EJ (4.99 quadrillion Btu), with coal being the leading

Figure 1. Growth of the world energy mix from 1990 and extrapolated to 2030 (data were extracted from the literature;[1] 1EJ = 0.9478 quadrillion Btu).

source at 39%, followed by oil at 37%, natural gas at 18%, other sources (wind, solar, etc.) at 6%, and without nuclear (0%).

Of the three largest energy sources (coal, oil, and natural gas), natural gas continues to be favored as an environmentally attractive fuel. Natural gas is arguably the cleanest fossil fuel.[2] In comparison to oil and coal, it emits virtually no sulfur, no solid waste, far less nitrogen oxide, and significantly less carbon dioxide than oil or coal. Furthermore, according to the U.S. Energy Information Administration,[3] new gas power plants required ∼50% of the levelized capital cost of coal per MWh, less than 33% the cost of nuclear, and less than 20% the cost of onshore wind, let alone offshore wind (Table 1). The direct greenhouse gas emissions from the combustion of coal and oil are also significantly higher per unit of energy compared to that of natural gas (Table 2) based on the carbon dioxide emission coefficients of the U.S. Energy Information Administration[4] and the review paper by Lim et al.[5] Within the next 15 years, many old coal-fired power stations will likely be retired, and if they are replaced with modern gas-fired power plants, emissions can be reduced by approximately 50% per unit of energy produced, as depicted in Table 2.

1.2. Importance of Liquefied Natural Gas (LNG) for Natural Gas Utilization. Although considered to be the most favored fossil fuel, natural gas faces the challenge of transport to the demand sites, because of its gaseous state. Pipelines and as LNG are the two most widely used methods for natural gas transport. An economic analysis by the Institute of Gas Technology (Figure 2, included in a report by the Center for Energy Economics in the University of Texas at Austin[6]) shows that transport of natural gas as LNG becomes cheaper compared to offshore pipelines for distances of more than 1290 km (∼800 miles) or 3540 km (∼2200 miles) in the case of onshore pipelines. Table 3 compares the fuel properties of
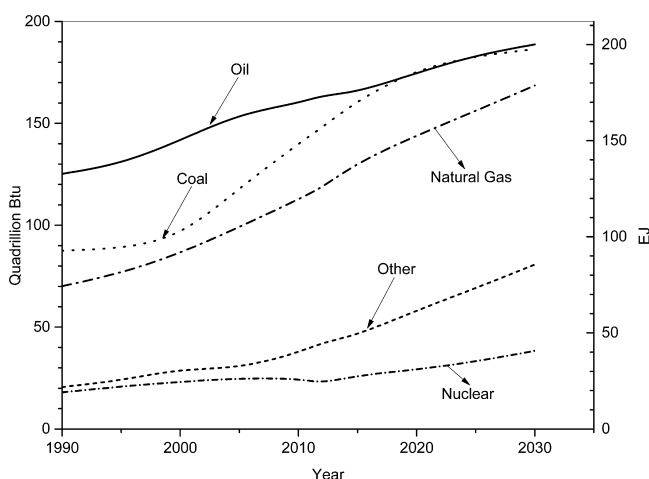
Table 1. Average Levelized Capital Costs of New Power Generation Resources[a]

energy source for the plant	levelized capital cost ($/MWh)	levelized capital cost ($/MMBtu)	total system capital cost ($/MWh)	total system capital cost ($/MMBtu)
natural gas	15.8–44.2	4.6–13.0	65.6–130.3	19.2–38.2
coal	65.7–88.4	19.3–25.9	100.1–135.5	29.3–39.7
nuclear	83.4	24.4	108.4	31.8
wind (onshore)	70.3	20.6	86.6	25.4
wind (offshore)	193.4	56.7	221.5	64.9

[a]Data were extracted and converted from the U.S. Energy Information Administration.[3]

Table 2. Emission of Air Pollutants from the Direct Combustion of Coal, Oil, and Natural Gas[a]

	carbon dioxide, kg/GJ (lbs/MMBtu)	nitrogen oxides, kg/GJ (lbs/MMBtu)	sulfur dioxide, kg/GJ (lbs/MMBtu)
coal	90 (210)	196 (457)	1114 (2591)
oil	71 (164)	210 (488)	482 (1122)
natural gas	50 (117)	40 (92)	0.3 (0.6)

[a]Data were extracted and converted from the literature.[4,5]
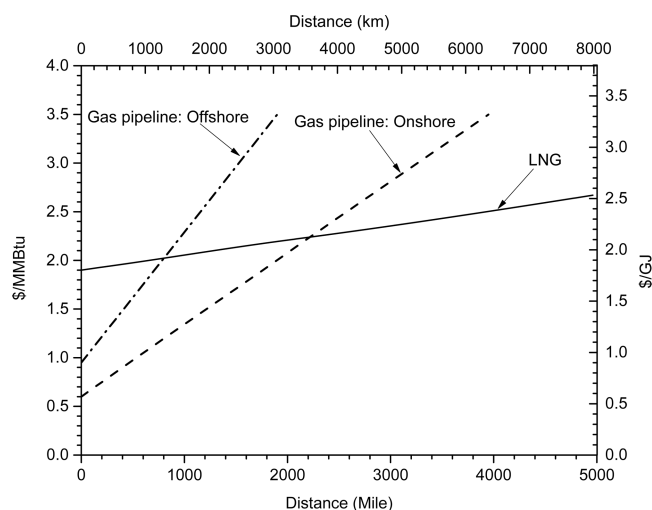
Figure 2. Transport cost of natural gas technologies relative to distance (data were extracted from the literature;[6] 1 $/GJ = 1.055 $/MMBtu).

natural gas at standard temperature and pressure (STP)[7−10] and LNG (−162 °C).[2,11−14] It can be seen that liquefaction of natural gas into LNG substantially increases the energy density of the fuel, enabling the economic long-distance transport of the fuel. Because international trade of natural gas is typically in distances exceeding 3540 km (~2200 miles), transport of natural gas as LNG is the preferred option. Therefore, LNG offers a global commodity, and its supply chain has been subjected to significant development in recent years as a result of concerns over increasing requirements on energy security, rising energy production costs, increasing natural gas prices, and rising gas import.[15] The global LNG trade has evolved from 73.62 billion cubic meters (bcm) [2.6 trillion cubic feet (tcf)] in 1990 to 283.17 bcm (10 tcf) in 2010 and is estimated to rise to 566.34 bcm (20 tcf) by 2040.[16] Another surge in the

Table 3. Fuel Properties of Natural Gas at STP[7−10] **Compared to Those of LNG (−162 °C)**[2,11−14]

properties	natural gas (STP)	LNG (−162 °C)
molecular weight (g/mol)	19.5	16.043
density (kg/m^3)	0.7–0.9	422.5
energy density (MJ/L)	0.0375	20.3
boiling point (°C)	−161	−161
viscosity (kg m^{-1} s^{-1})	1.1×10^{-5}	1.14×10^{-4}
surface tension (N/m)		13.36
specific heat (kJ kg^{-1} K^{-1})	2.215	4.186
thermal conductivity (W m^{-1} K^{-1})	0.033	0.2015
shelf life (day)		5−7

LNG trade is expected to come in the time frame of 2015−2025 because of projects in Australia expected to be completed in 2020, closely followed by the completion of projects in North America.[16] Some key LNG projects worldwide are presented in Table 4.[17−25]

Technological advances have significantly increased the profitability of LNG value chains,[26] leading to a substantial reduction in the cost of LNG value chains by 30−50% between the 1980s and 2003.[27,28] For the total capital cost, the average breakdown is ~21% for assets in upstream exploration and production, ~40% for liquefaction plant, ~20% for shipping facilities, and ~18% for storage and regasification terminals.[5,29] Concrete values depend upon different factors, including traded volume, transportation distance, and/or employed technologies. Table 5 shows the typical investment of an 8 mtpa LNG process.[28,30] The upstream gas prices mainly depend upon the reservoirs, while the liquefaction cost depends upon feedgas composition and the liquefaction process in use. The shipping costs are determined primarily by the distance between the sellers and buyers, while regasification prices are dependent upon the construction costs, regasification technology, and storage capacity.[28]

1.3. Life Cycle Performance of Natural Gas and LNG. The life cycle performance of coal (underground and surface mining),[3,31,32] natural gas (conventional and shale gas),[3,31−33] oil (crude and oil sands),[31−33] and biofuel[3,32−34] energy systems for a life period of 20 year is presented in Table 6. It can be seen that, of the total greenhouse gas (GHG) emissions in the life cycle assessment (LCA) of the energy systems, approximately 91, 95, and 79% for coal, oil, and natural gas, respectively, are released during the downstream combustion. Additionally, on average, emission during fuel production is 3% lower for oil and 21% higher for coal when compared to natural gas. This is mainly due to the high emissions during the fuel combustion stages in the coal system. It is noted that biofuels can be produced from a wide range of sources, and as a result, obtaining an average comparison of emissions to that of the fossil fuels is quite challenging.

A similar trend is also observed in the electricity production analysis, in which coal and oil on average produce more emissions than natural gas; however, fossil fuels, in general, produce more emissions than biofuels. It is important to note that the emissions from electricity production for biofuels (Table 6) did not consider carbon emissions from land use/management, and most studies do not include the CO_2 emission from biomass plants, with the assumption of CO_2 emitted being equal to CO_2 absorbed in biomass growth stages.[32] Because the main area of use for biofuels is in transport, biofuels have low GHG emissions per kilometer

Table 4. Some Key LNG Projects Worldwide[17−25]

project	country	capacity (mtpa)	number of trains	status
Darwin LNG	Australia	3.7	1	operating
Brass LNG	Nigeria	10.0	2	operating
Venezuela LNG	Venezuela	14.1	3	operating
Trinidad and Tobago	Trinidad	15.7	4	operating
North West Shelf	Australia	17.1	5	operation
Arzew	Algeria	17.3	3	operating
Bontang LNG	Indonesia	22.2	8	operating
Nigeria LNG	Nigeria	22.2	6	operating
Qatar gas 1−4	Ras Laffan	41.2	7	operating
Gladstone LNG	Australia	7.2	2	under construction, 2015
Ichthys LNG	Australia	8.4	2	under construction, 2016
Yamal LNG	Yamal	16.5	3	under construction, 2018

Table 5. LNG Value Chain Costs for a Typical 8 mtpa Process[28,30]

	upstream	liquefaction	shipping	regasification	total
gas use	nil	10−14%	1.5−3.5%	1−2%	12.5−19.5%
capital expenditure (billion dollars)	$2−6	$6−10	$1−2.5	$1−1.5	$10−20
miscellaneous (operating cost, maintenance cost etc.)		5−7% of capital cost		3−4% of capital cost	
unit cost per GJ ($/MMBtu)	$0.95−2.84 ($1−3)	$2.84−4.27 ($3−4.5)	$0.76−1.42 ($0.8−1.5)	$0.38−0.76 ($0.4−0.8)	$4.93−9.29 ($5.2−9.8)

Table 6. LCA of Different Energy Sectors for a 20 Year[a] Period[3,31−34]

	coal	natural gas	oil	biofuel
fuel produced[b] (g of CO_2 equiv/MJ)	110−130	90−101	97−116	68−131
electricity produced[b] (g of CO_2 equiv/kWh)	675−1689	290−930	510−1170	18−360
transport[b] (g of CO_2 equiv/km)		155−185	185−220	15−195
total system levelized cost ($/MWh)	100.1−135.5	65.6−130.3		111.0

[a]The 20 year period was chosen because of the global warming potential of the specified fuel sources within that time frame. [b]The GHG emission is the total GHGs released during the development of the infrastructure, production/procurement of the fuel, and combustion of the fuel.

traveled in a passenger car, closely followed by natural gas, and then oil with the highest GHG emissions. Overall, the LCA analysis in Table 6 shows that natural gas on average produces low GHG emissions for fuel production, electricity production, and transport use and costs less as a system compared to other fossil fuels, such as oil and coal. This makes natural gas a very strong competitor in the world energy sector. While the GHG emissions for biofuels are considerably lower than those of the fossil fuels, the biofuel sector is in its infant stage and there is still a long way for its growth to make a significant contribution to the world energy mix.

In comparison to pipeline gas, LNG results in a ~50% increase of GHG emissions as a result of additional liquefaction and tanker transport, according to the LCA analysis by Jaramillo et al.[35] presented in Table 7. It is noted that the

Table 7. LCA of LNG versus Pipeline Transport[a]

	emission intensity (g of CO_2 equiv/kWh)	
stages of life cycle	LNG	pipeline (natural gas)
fuel production	109	109
liquefaction	68	N/A
transport	27	N/A
regasification	5	N/A

[a]Data were extracted from the study by Jaramillo et al.[35]

emission as a result of leakages from the pipeline transport method was neglected. It was further reported that, over the years, various technologies used in LNG value chains result in an energy efficiency ranging from 60 to 90%.[30,36] The two most important methods of improving efficiency are by improving the efficiency of the heat exchanger or that of turbomachinery.

1.4. Objectives and Outlines of This Review. Considerable recent research was conducted in developing efficient LNG value chains and managing the associated risks, such as those in handling, storage, and transport of LNG. This has been largely driven by the rapid increases in production and use of LNG, potential terrorist threats, and public confidence in LNG safety. The potential hazards include cryogenic tissue damage and embrittlement of material. Such hazards can be potentially caused by various physical and chemical interactions with LNG via direct contact, pressure from rapid phase transitions (RPTs), asphyxiation, deflagrations, detonations, LNG vapor cloud fires, and LNG pool fires. Upon a LNG spill, a LNG pool forms on the substrate and vaporizes rapidly as a result of the local mixing and heat transfer. Ignition of the LNG pool (LNG pool fire) or the LNG vapor cloud (vapor cloud fire) both affect the vaporization/dispersion process and create thermal hazards. Table 8 summarizes some of the reviews in the literature[5,15,37−41] on different aspects of the LNG value chains. It can be seen that the existing reviews related to LNG

Table 8. Some Published Review Papers Regarding Different Aspects of the LNG Value Chain

reference	literature covered	years covered	aspects covered
Wood[15]	outlook of the global LNG trade	up to 2012	current status and future growth of global LNG
Lim et al.[5]	LNG plant designs	up to 2012	available LNG plant designs and implemented designs and their optimizations in practice based on costs
Luketa-Hanlin[37]	studies on large-scale LNG spills	up to 2006	behavior of LNG spill, including combustion and development of predictive models, concluding that experiments on the order of 100 m^2 are required
Cleaver et al.[38]	summary of experimental data on LNG safety	up to 2006	behavior of LNG spill, combustion, and modeling issues, concluding that more experimental studies of RPT are required
Koopman et al.[39]	LNG safety research	up to 2006	behavior of LNG from research performed by Lawrence Livermore National Laboratory, including dispersion model development
Raj[40]	LNG fires	up to 2006	some LNG fire experiments on land and water from the 1970s to 1980s are reviewed, including fire hazard prediction models
Havens and Spicer[41]	problems with the United States LNG siting regulations	up to 2006	problems with determining and specifying exclusion zones for LNG spills

production and the events following a LNG spill were all done up to 2006.

Therefore, this review focuses on some recent research advances in LNG production, spill, dispersion, and safety from 2007, although the classic earlier literature will also be covered to maintain a smooth connection to prior knowledge in a logical flow. The structure of this review is organized as follows: Section 1 is a brief introduction of LNG and the need of this review. Section 2 presents an overview on the LNG production process, covering upstream gas production and gathering, liquefaction, shipping, and regasification processes. Some recent developments in the optimization of LNG plants are also included. Section 3 summarizes the recent advances in experimentation and modeling of LNG spills, covering the events following a LNG spill, including LNG pool formation, vapor dispersion, and combustion. Section 4 presents the methods of improving the safety of personnel, facilities, and ships with a direct correlation to regulations, such as U.S. Department of Transportation (DOT) Regulations, 49 Code of Federal Regulations (CFR), National Fire Protection Association (NFPA) 59A standard, and International Gas Carrier (IGC) code. The key findings and future research perspectives are then outlined in Section 5. The review is then concluded with overall concluding remarks in Section 6.

2. LNG PRODUCTION CHAIN

A LNG production chain transforms the raw natural gas into LNG as a carrier product for the transport and distribution of natural gas to the end users. It consists of four crucial stages, including upstream gas production and gathering, liquefaction, shipping, and regasification. Below is a brief overview on these four stages, including some recent research and development (R&D) advances in these aspects.

2.1. Upstream Gas Production and Gathering. All fossil fuels are formed when remains of plants, animals, and microorganisms are compressed underneath the earth under high pressures and temperature for long periods of time. The suitable geological conditions breaks down the carbon bonds in organic matter to form natural gas, oil, or coal, with more oil produced at lower temperatures but more natural gas produced at higher temperatures.[42] Natural gas is normally trapped under ground in a reservoir (conventional gas) or by sedimentary rock (shale gas) and, at times, interacts and is absorbed by coal (coal seam gas).[43] It can be found onshore or offshore, as associated gas or non-associated gas.[28] The non-associated gas can be dry, meaning that it is composed of purely methane, or it

Table 9. Typical Composition of Natural Gas Compared to LNG[44]

component (mol %)	natural gas	LNG
H_2S	0.96	
CO_2	2.45	
N_2	3.97	0.00−1.00
CH_4	82.62	84.55−96.38
C_2H_6	4.84	2.00−11.41
C_3H_8	1.78	0.35−3.21
i-C_4H_{10}	0.39	0.00−0.70
n-C_4H_{10}	0.67	0.00−1.30
i-C_5H_{12}	0.29	0.00−0.02
n-C_5H_{12}	0.27	0.00−0.04
n-C_6H_{14}	0.34	
others	1.42	
total	100.00	100.00

could be wet, containing hydrocarbons, such as butane, propane, and other condensates. Associated gas on the other hand is very expensive to gather for sale, and as a result, it is flared.[28] Table 9 lists the typical composition of a sample of natural gas taken from Qatar's North Field.[44]

All forms of natural gas need to be treated to remove impurities (e.g., carbon dioxide, hydrogen sulfide, nitrogen, and mercury) and/or heavier hydrocarbons (e.g., butane and propane) before the gas can be sent to the downstream liquefaction plant. The pretreatment may consist of three main stages: acid gas removal, dehydration, and mercury removal (Figure 3).[45] Impurities in the gas stream are referred to as acid gas, and removal of this acid gas can be achieved via using an amine solvent mixed with water.[46] If significant hydrogen sulfide is present in the acid gas, then a separate stream for sulfur recover is required.[28] Gas leaving the acid gas removal system is generally saturated with water vapor and, therefore, passed through a dehydration system. This is to prevent freezing when the gas reaches the main liquefaction exchanger and attained by first cooling the gas with water, air, or a refrigerant and then passing it through a molecular-sized sieve.[6] The final stage of gas pretreatment is mercury removal. Mercury can corrode aluminum, and because most equipment in the heat exchanger is made from aluminum, it is crucial that this process is carried out.[46] Mercury removal is achieved by passing the feed gas through a sulfur-impregnated carbon bed, during which the mercury becomes a non-volatile mercury sulfide.[46] The natural gas after this series of pretreatment is then sent to the liquefaction plant.
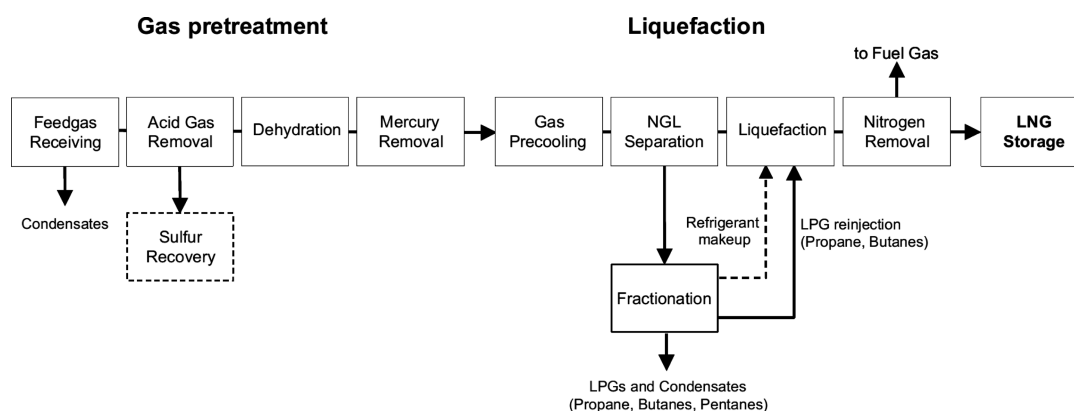
Gas pretreatment | **Liquefaction**

Figure 3. Natural gas pretreatment and liquefaction (adapted from the literature,[45] NGL = natural gas liquid, LPG = liquefied petroleum gas).

Table 10. Commonly Used LNG Liquefaction Processes[a]

process	developer(s)	single train capacity (mtpa)	efficiency relative to cascade	efficiency relative to C3MR
Phillips' optimized cascade (POC)	ConocoPhillips	4–9	1.00	1.16
PRICO	Black and Veatch Pritchard	0.1–2.1	1.25	1.19
APCI propane precooled mixed refrigerant (C3MR)	APCI	0.5–6.1	1.15	1.00
Shell and APCI dual mixed refrigerant (DMR)	Shell and APCI	0.5–8.4	N/A	1.03
IFP/Axens Liquefin	IFP/Axens	N/A	N/A	N/A
parallel mixed refrigerant (PMR)	Shell	6–9	N/A	N/A
Gaz de France integral incorporated cascade (CII)	Gaz de France	N/A	N/A	N/A
APCI AP-X	APCI	5.8–9	N/A	N/A
Statoil–Linde mixed fluid cascade (MFC)	Linde in collaboration with Statoil	4–6.6	N/A	N/A

[a]Data were extracted from the study by Lim et al.[5] that was based on the literature.[49–70]

Table 11. Comparison of Refrigeration Cycle Configurations[a]

	refrigerant			heat exchanger		
process	precooling	liquefaction	subcooling	precooling	liquefaction	subcooling
POC	propane	ethylene	methane	plate fin heat exchanger (PFHE) or core-in-kettle	PFHE	PFHE
PRICO	mixed refrigerant (MR)			cold box (PFHEs)		
C3MR	propane	MR		core-in-kettle	coil-wound heat exchanger (CWHE)	
DMR	MR	MR		CWHE	CWHE	
Liquefin	MR	MR		PFHE	PFHE	
PMR	propane or MR	parallel MR				
CII	MR			heat-exchanger line (two PFHEs)		
AP-X	propane	MR	nitrogen gas	core-in-kettle	CWHE	CWHE and PFHE
MFC	MR	MR	MR	PFHE	CWHE	CWHE

[a]Data were extracted from the study by Lim et al.[5] that was based on the literature.[49–70]

2.2. Liquefaction and Storage. The natural gas leaving the production facilities is piped to a liquefaction plant, which can be located onshore or offshore (to date, most liquefaction plants have been onshore), and may have a number of parallel systems (called trains) of heat exchangers and gas or steam turbines driving the compressor.[28] The natural gas is liquefied into LNG via cooling it to 112 K,[47] reducing the volume of natural gas by a factor of 600. The LNG product is then stored in insulated double-walled tanks designed to maintain the low temperatures of the LNG. These storage tanks contain an inner cryogenic nickel/steel tank, surrounded by insulation and then followed by a pre-stressed concrete or mild steel outer tank (when mild steel is used as the outer tank, a berm is constructed to contain the LNG in the case of a spill).[28]

The rising demand of LNG has led to the development of the gravity-based structure (GBS) and the floating LNG (FLNG) concepts aimed at exploiting offshore natural gas reserves that are too remote or not economically viable for onshore liquefaction facilities.[48] Essentially, the GBS is an artificial island, where LNG production and storage will take place, and is intended for shallow waters. In the case of FLNG, the system is floating and mobile, unlike the GBS. The idea is that the structure will be prefabricated onshore and sunk to the seafloor at the required location. This technology has been

applied to multiple oil production facilities.[48] However, such LNG facilities also suffer from some undesired disadvantages, including large footprint, large construction costs, constant upgrading for existing onshore facilities, only applicable to a smaller range of water depths, and potential safety risks (requiring a safe mechanism for transferring LNG into LNG tankers).[28]

Various liquefaction processes have been developed by different companies, as reviewed in a recent publication[5] and also summarized in Tables 10 and 11.[49−70] The fundamental principles of these processes can be found in other related publications by Barron,[71] Walker,[72] or Timmerhaus and Flynn.[73] As shown in Tables 10 and 11, these processes have different single train capacity and efficiency (relative to cascade or C3MR) and deploy a range of refrigerants and heat exchangers for precooling, liquefaction, and/or subcooling.

The recent research advances on the topic has been focused on the optimization of the LNG liquefaction process, via several possible strategies:

Design or Selection of Optimized Refrigerant Mixture. Alabdulkarem et al.[74] use a generic algorithm (GA) method from MATLAB in combination with HYSYS to design an optimized refrigerant mixture for a C3MR LNG plant, achieving a total reduction of over 9% in power consumption. The method can be applied with confidence for a global optimum, unlike the previous method by Michelsen et al.[53] As shown in Figure 4, it is also more efficient than the previous
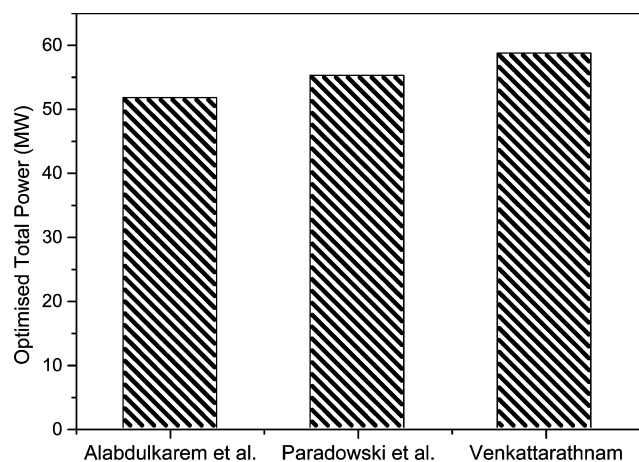
Figure 4. Optimized power consumption by Alabdulkarem et al.[74] compared to the methods by Paradowski et al.[75] and Venkattaratham[76]

methods (e.g., by Paradowski et al.[75] and Venkattaratham[76]) for propane precooled refrigerant optimization processes. However, the method provided by Alabdulkarem et al.[74] incorporates numerical algorithms without including process knowledge, such as knowledge of the boiling point differences of MR components, MR component distribution curves, and specific refrigeration effect of bringing a MR system closer to reversible operation. Khan et al.[77] therefore proposed a knowledge-based optimization (KBO) method for selecting mixed refrigerant, which achieved a total reduction in power of 30 and 13% in the SMR and C3MR LNG processes, respectively. Although a global optimum cannot be achieved from the KBO,[77] it is quite robust and can result in a higher energy saving than other methods, such as that provided by Alabdulkarem et al.[74]

Optimization of the Precooling Cycle. Via HYSYS simulations, Castillo et al.[78] have recently concluded that a three-stage propane precooled cycle can be more sufficient than a mixed refrigerant cycle. However, in cool climates (6 °C), the reduced power share from the three-stage propane precooled cycle results in the mixed refrigerant cycle as a preferred alternative.
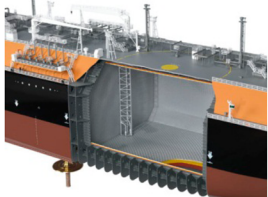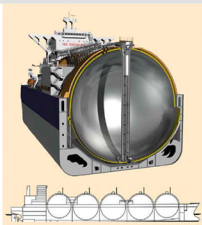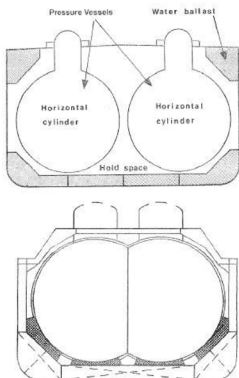
Utilization of Process Energy. Conventional optimization of the LNG liquefaction process focuses on component replacement that requires significant modifications to existing process licenses and becomes difficult and expensive for integration into the existing facilities. Recent research progress has been made on the smart use of process energy that can be easily implemented into existing facilities for improving the efficiency of the LNG liquefaction process. For example, the cold exergy of subcooled LNG can be used to recondense the light component of LNG after it has passed through a phase separator, leading to reduction in the pumping power of vaporized natural gas and, hence, the whole liquefaction process.[79] The energy of the flash gas can also be used for cooling the natural gas and refrigerant and, hence, reducing the specific power to various extents, depending upon the ratio of the natural gas feed rate to LNG flow rate.[80] Another method is to use gas turbine and/or waste heat power for the subcooling of the propane cycle (after the condenser by 21 °C), leading to 13 and 23% increases in the process performance coefficient and total cooling capacity, respectively.[81]

Development of Numerical Methods for Optimization. Recent research advance demonstrates that quadratic sequential programming (via the use of a Fortran code NLPQLP, coupled with HYSYS) can drastically improve the calculation efficiency in the optimization of LNG processes (in particular, the PRICO process).[82] The method produced results within 1% of the optimal value and carried out simulations in 2−6 min compared to the typical 4−22 h of other methods.[82] The method is proven to be accurate and efficient for a simple LNG process, although its application to more complex LNG processes is yet to be assessed because of more difficulties in the coding process and the linking between NLPQLP and HYSYS. In addition, thermodynamic analysis, mathematical programming, and rigorous simulations were used by Wang et al.[83] to develop a new methodology for LNG liquefaction process design and operation optimization. This method was able to achieve a total power saving of 13% (higher energy saving than that by Alabdulkarem et al.[74]) for a C3MR LNG plant and was shown to be able to reach a global optimum.

Deployment of New Control Strategies. A recent study by Michelsen et al.[53] demonstrates that the use of a set of non-constant control variables rather than the standard "constant-set-point" policy can reduce the operation losses (by up to 98%) because of the changes in unknown disturbances and other uncertainties. The disadvantages of such a non-constant control variable method are the trial and error approach for selecting the non-constant control variables, requirement of recalculations upon changes in process constraints, and no guarantee in reaching a global optimum.

Considerations of Thermal Interaction between Streams. Multi-stream heat exchangers, consisting of two hot streams (high-pressure mix refrigerant and natural gas feed) and a cold stream (low-pressure mixed refrigerant), are usually optimized by using commercial software, such as HYSYS and SIMSCI PRO II.[84] In process analysis, these commercial software assume that the two hot streams are at the same temperature.

Table 12. Summary of Various Cargo-Containing Systems for LNG[89−92]

Type	membrane	Moss	IHI SPB	Cylindrical
appearance	source: BG Group	source: LNG World Shipping	source: FLEX LNG	source: TGE Marine
classification	integrated tanks	independent tanks (Type B)	independent tanks (Type B)	independent tanks (Type C)
sub-types	GTT No. 96 GTT Mark III GTT CS1 membrane double row	-	-	cylindrical design bilobe design
designed vapour pressure	less than 70 kPa	less than 70 kPa	less than 70 kPa	greater than 200 kPa
capacity	145,000–265,000 m³ (4–5 cargo holds)	138,000–255,000 m³ (4–5 cargo holds)	87,500 m³ (4 cargo holds)	2,500–30,000 m³ (2–4 cargo holds)
self-supporting tanks	no (reacts with hull structure)	yes (independent of hull structure)	yes (independent of hull structure)	yes (independent of hull structure)
tank material	36% nickel steel (Invar) stainless steel	aluminum alloy of 9% nickel steel	aluminum alloy of 9% nickel steel	aluminum alloy of 9% nickel steel stainless steel
insulation properties	530 mm insulation plywood boxes filled with perlite 250–270 mm reinforced polyurethane foam	220 mm polyurethane foam	polyurethane foam	300 mm polystyrene panels
secondary barrier	full secondary barrier	partial secondary barrier	partial secondary barrier	no secondary barrier
ability of partial filling	tanks are to operate at below 10% or above 80% of tank depth; to reduce sloshing	no limits as spherical tank shape prevent sloshing	no limits as centreline bulkhead prevents sloshing	no limits as tank shape prevent sloshing
deck space	flat deck space with chamfer	very limited deck space	plenty of deck space	plenty of deck space
maintenance on site	poor accessibility to tanks and requires staging	-	excellent accessibility to tanks	-
ships in serves	∼ 230	∼ 100	2	-

Via energy balances, of differential equation, Chang et al.[84] was able to show that the assumption made by commercial software is unrealistic. The assumption can only be achieved if the product of the heat-transfer coefficient and heat-exchanger area (UA) between a hot/hot stream (hot stream in contact with a hot stream) is greater than that of a hot/cold stream (hot stream in contact with a cold stream).[84] Chang et al.[84] was also able to show that for any total UA, there is an optimal ratio of UA between the streams to increase performance, and any

direct contact (heat-exchanger tubes) will deteriorate performance.

Improvements via LNG Plant/Process Evaluations. An exergy evaluation of a LNG plant in Norway[85] concludes that 37% of the overall exergy losses are due to the process plant, 52% of the overall exergy losses are from the combustors and gas turbines, and 11% of the overall exergy losses are from the exhaust gas (stack exhaust). Ambient temperature analysis also shows that a cooler climate will reduce the total exergy required for the liquefaction process. Improvement of the exergy
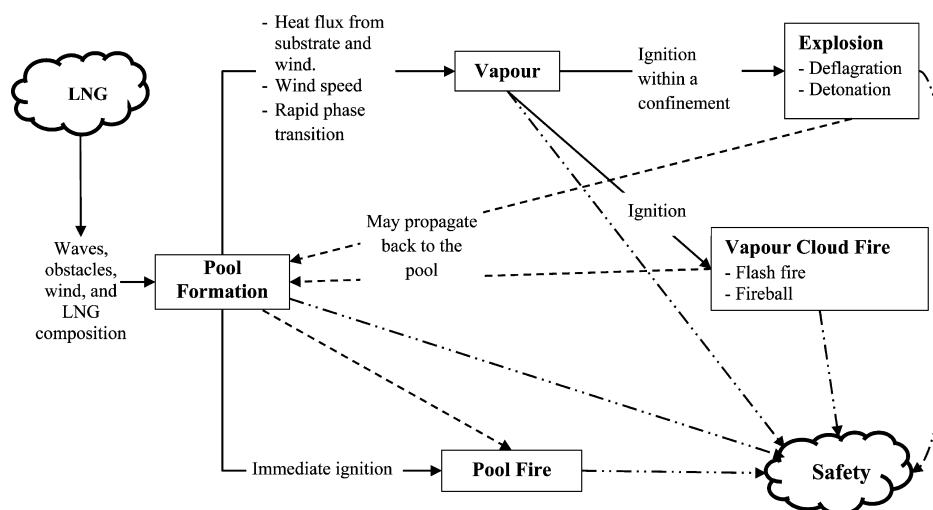
Figure 5. LNG spill events.

efficiency can be achieved via a generic algorithm optimization method developed by Li et al.[86] While the exergy efficiencies of current large-scale processes are about 41−45%, the exergy efficiency can be increased up to 58% for methane liquefaction.[86] Of the three main options for offshore associated gas liquefaction resources, a comparative analysis[87] showed that the nitrogen expander process has higher power consumption (52−68%) and poorer economic performance than the C3MR or MR process. The nitrogen expander process appears to be more suitable for offshore processes because of its simplicity, compact design, less sensitivity to floating production storage and offloading, higher safety, and operability.[87]

In addition, after liquefaction, LNG is stored in storage tanks before been transferred into a LNG tanker for transport. In comparison to several conventional LNG storage models, a recent model[88] based on normal equations applied to nonlinear parameter estimation has significantly improved the modeling accuracy for safe and economic managing of LNG storage sites (prevent stratification and rollover of LNG). The model also converges faster to a heat- and mass-transfer coefficient and can be used with level−temperature−density profiles (which can easily be obtained from gauges on the storage tanks) to obtain the required results.[88]

2.3. Shipping. After liquefaction and storage, the LNG is then loaded onto specialized ships for its long-distance transport. The ships are designed with double hulls for structural rigidity and also to provide room for ballast water, considering how light the cargo is. The cargo tanks are not a part of the ship structure and are therefore installed separately into the holds of the ship.

Table 12 lists the features and characteristics of four types of LNG ships that have been developed since the late 1960s.[89−92] The membrane-type ships, ranging in size from 145 000 to 265 000 m³, use fully integrated rectangular tanks with reinforced polyurethane or plywood/perlite insulation.[90] With regard to its close competitor, the moss-type ships, ranging in size from 138 000 to 255 000 m³, are designed with spherical tanks, independent of the hull structure, and use polyurethane insulation.[90] There is a preference for the membrane tankers, mostly because of their capacity efficiency (use of the hull shape), with little to no void space between the storage tanks and the ballast tanks compared to the moss tanker.[28] This will make a moss tanker of similar capacity as the membrane tanker

more expensive. However, the moss tanker has a higher resistance to sloshing and will most likely be considered for future offshore storage, especially in areas of bad weather. Next is the IHI SPB-type ships that also use rectangular tanks with polyurethane insulation; however, unlike the membrane-type tanks, the IHI SPB does not rely on the hull of the ship for structural support.[91] The IHI SPB ships are also resistant to sloshing, but its expensive design and small capacity (87 500 m³) compared to that of the membrane or the moss systems explain why only two ships are currently in-service. The last type is the type C (cylindrical) system. The type C ships are able to resist sloshing, use polystyrene for insulation, and were designed specifically for cases where small-cargo transportation is required (2500−30 000 m³).[90]

During the shipping of LNG, boil-off occurs (approximately 0.15% of the cargo[28]). Because current LNG ships are not constructed with an on-board regasification facility, the boil-off gas is captured and used as fuel to assist in propelling the ship. Once at the import terminal, the LNG is unloaded, leaving behind a small amount of LNG, the heel, to keep the tank cool in the ballast voyage.[28] To date, there has been no LNG cargo lost or spilled during the shipping phase, and it is believed that, with acceptable maintenance, the LNG vessels can have a working life of 40 years or more.[28]

2.4. Regasification Terminals. A LNG value chain ends with regasification terminals. At each unloading berth, several unloading arms, with articulated joints and emergency release couplings, are generally employed for transferring LNG from the LNG tankers to the storage tanks. The main purpose of storage tanks is to hold the LNG until it is ready to be vaporized. The storage tanks used at the regasification terminals are exactly the same as those at the liquefaction plant.[28]

The LNG is then passed through vaporizers, which warms the LNG to or above 5 °C (41 °F). The vaporizers use either seawater, air, natural gas, or an external heat source in the vaporization process of LNG and consume a significant amount of electrical energy. Using a new combined power cycle that incorporates a gas turbine and an ammonia cycle with one pressure step, the efficiency can be improved from 44 to 46% while decreasing capital cost.[93] Because LNG is a cryogenic liquid, boil-off occurs at about 0.05% per day of tank volume or less. To decrease boil-off gas (BOG), it is believed that the number of stages (compression and reliquefaction) in the

regasification system should be increased, because an increase in the number of stages leads to a decrease in the BOG flow rate.[94] Although this will reduce the operation cost, it will also increase the total capital cost; therefore, an optimum number of stages will need to be determined (via optimization using models, e.g., developed by Liu et al.[94]).

Cold is also an important energy source that is available during regasification. Innovative technologies, such as a novel cogeneration concept, have been proposed to recover exergy from LNG for the generation of power (with an overall system efficiency of 52%).[95,96] There is potential for this novel cogeneration concept to be improved by focusing on the gas turbine power system, to improve efficiency, reduce environmental impact, and improve cost.[97] Other innovative technologies using cold energy consider the use of helium (49% efficiency),[98,99] ammonia−water mixture (48% efficiency),[100] and a combination of tetrafluoromethane and propane (23.5% efficiency)[101] as a working fluid, with some plants even able to achieve near-zero CO_2 emission.[102] The feasibility of using cold energy from LNG regasification in other industries, such as deep freezing agro-food industries and air-conditioning facilities in supermarkets and hypermarkets, has also been demonstrated in numerous literature, with carbon dioxide as the preferred fluid for transferring the cold energy.[103−106]

After LNG regasification and prior to any natural gas leaving the regasification terminal, it is metered, during which its pressure and quality is regulated to meet customer specifications; at times, the natural gas is odorized to help identify leaks in transportation systems or customer appliances.[28]

2.5. LNG Value Chain Potential Hazards. During the LNG production processes, some simple failures/events can lead to a series of catastrophic events, with the most common been a LNG spill. The block flow diagram in Figure 5 shows the likely events that can follow, after a LNG spill. The factors and parameters that influence and control the spread of these events are not fully understood. The events in Figure 5 can be categorized into three main areas of interest: (a) pool formation, understanding is needed on the key factors that affect the pool spreading, pool boiling, and occurrence of RPTs; (b) vapor dispersion, understanding is needed on what effect wind and obstacles have on the dispersion processes of the vapor cloud and there other governing factors; and (c) combustion, understanding is needed on the characteristics of (and the key factors that influence) the pool fire and vapor cloud fire formation and spreading, and how the two different fires compare to each other. These types of questions have led to the use of experimentation and mathematical modeling to study LNG spills, with the aim of improving knowledge and further understanding the likely case of events following a LNG spill and how it can be prevented and/or managed. Such knowledge and understanding are essential to maintaining and managing the safety of LNG.

3. LNG SPILL, VAPOR PRODUCTION, DISPERSION, AND COMBUSTION

Experimental studies of LNG vapor production, dispersion, and combustion commenced from the early 1970s at both lab and field scales.[38] These investigations were carried out with the main objectives of collecting experimental data for benchmarking and the validation of computer models.[107] Extensive measurements were conducted considering various parameters, including meteorological parameters (e.g., temperature, humid-

ity, wind speed, turbulence, solar heat flux, etc.) and gas parameters (e.g., temperature, concentration, ground heat flux, etc.).[38] Spills of LNG, on either land or water, can range from all sizes. At times, the anticipated spill size or conditions cannot be replicated experimentally, and this has led to the use of mathematical models to simulate, study, and understand the characteristics of a LNG spill, leading to vapor production, dispersion, and/or combustion. These mathematical models would primarily need to be validated, with existing experimental studies, to be confident in using them for further studies.

While the overall research progress is briefly summarized, this review emphasizes the recent experimental and modeling development since 2007 on these important aspects. Section 3.1 presents a summary of pool formation and factors affecting this process, followed by a recently developed mathematical model, to allow for better prediction of the shape and behavior (up to dispersion) of a LNG pool following a spill. Section 3.2 summarizes the vapor dispersion process, including what parameters drive this process and the mathematical models used in studying vapor dispersion. Section 3.3 contains a summary of LNG fires, including the modeling methods of LNG pool/vapor cloud ignition, in effect of studying overpressures and radiant heat flux that would arise.

3.1. Pool Formation. Upon spilling on water, LNG spreads and boils because of the temperature difference between LNG and the water surface. Spills on confined, calm water can become similar in behavior to spills on land, because of ice formation, which will result in a decrease in the evaporation rate over time. The vaporization rate is also important in that it influences the distance to the low flammability limit (LFL) and the burn rate of pool fires. Therefore, the vaporization rate and the size and shape of the LNG pool are key parameters influencing LNG pool formation.[37]

3.1.1. LNG Spreading on Water. In the literature, most of the experiments concerning LNG spreading on water were conducted prior to 2007. Those experiments were on small scales, and application of such experiments results to large-scale applications are known to have the main technical uncertainties in terms of the dynamics of the front of the spreading pool and the heat-transfer rate.[37] While efforts were made to deploy models for simulating bubble formation at large scales based on small-scale experimental data, the effect of waves and ice formation can introduce some more uncertainties in such predictions.[38] Therefore, large-scale experiments are certainly still in need.

3.1.2. Pool Boiling. Pool boiling occurs when LNG is spilled on water through three stages, namely, nucleate boiling, transition boiling, and film boiling. The up-to-date R&D on pool boiling of LNG leads to several major conclusions:[37,108] (a) evaporation is a function of the molecular weight of the material (starting from the lowest); (b) boiling does not take place at a constant temperature; (c) the vaporization rate of LNG is very different from that of pure methane, and the addition of ethane or propane results in a more rapid vaporization at increased boil-off rates by a factor of 1.5−2; and (d) evaporation during the spill phase is also an important consideration because it may contribute to up to 20% of the overall evaporation.

3.1.3. RPTs. RPTs can be classified as physical or mechanical expansion, in which high-pressure energy is released, and occur when cold LNG comes into contact with water. RPTs occur primarily during the experiments at laboratory scale.[37] The only large-scale RPTs observed were during the Coyote test series,

Table 13. Some Well-Known Pool Formation Models for LNG Pool Modeling

	LNG pool formation models			
model	SOURCE5[41,111−113] integral model	GASP[114,115] integral model	PHAST[118−122] integral model	LNGMAP[11,126,127] integral model
principles	initiated in the 1980s and simulates instantaneous or continues releases, pool formation, and evaporation	initiated in the 1980s and simulates instantaneous or continues releases of a circular pool and vaporization rate	initiated in 2002 and simulates discharge, pool formation, evaporation, dense gas dispersion, and fires	initiated in 2005 and simulates instantaneous or continues releases of a circular pool, vaporization rate, and fires for marine spills
method	algebraic equations and, in some cases, are solutions of ordinary differential equations	algebraic equations and, in some cases, are solutions of ordinary differential equations	algebraic equations and, in some cases, are solutions of ordinary differential equations	discrete set of linked algorithms and a particle-based approach
accuracy	models bulk quantities as a function of time	models bulk quantities as a function of time	pseudo-component approach for mixtures	fully integrated geographic information system
validations	unclear, although it might have been validated in the process of validating DEGADIS	some validations were conducted during the development of the program but most were not published	wind tunnel experiments; Kit Fox; numerous field experiments	can range from 1 to 38%; however, no large-scale experiments are available to be used for validation; ABS Consulting and Sandia numerical simulation cases
advantages	output from SOURCE5 can be used as input to the DEGADIS dispersion code; can model LNG spreading on land, confinement by a simple shape bund/dike, instantaneous or continuous releases, drainage and permeable ground; can also model LNG spread on water for both instantaneous and continuous releases; accounts for heat conduction from substrate	can account for spills on land and water; can model LNG spreading on land, confinement by a simple shape bund/dike, instantaneous or continuous releases; accounts for smooth and rough ground; heat transfer from the sun, substrate, and air are all included	can account for spills on land or water surfaces; accounts for instantaneous and continuous releases; effects of bund walls; can model heat conduction from the substrate, convection from the air, and radiation	can model pool spreading, transport on water, evaporation from water, and the transport in the atmosphere; either constant or time dependent; accounts for thermal effects of conduction and radiation
disadvantages	cannot model a rough or slopping ground; cannot model non-circular pools, channeled flows, or confinement by arbitrarily shaped dikes; heat transfer from the sun, fire, and air are all neglected; inability to account for mixing with air in a confinement; inability to account for expansion of the vapor volume because of heating above the boiling temperature	permeable ground, sloping ground, and drainage are not modeled; does not account for non-circular pools; radiative heat from fire is not included but can be added as user-defined input; does not account for RPTs	cannot model non-flat ground	cannot account for RPTs; restricted to marine spills (spills on a water surface)
scales	field; laboratory	field	field	field
applications	LNG hazard assessment	LNG hazard assessment	hazard analysis (power plants, refineries, chemical plants, petrochemical plants, pharmaceutical facilities, and oil rigs)	hazard analysis (LNG ships and offshore platforms)
code accessibility	N/A	N/A	N/A	N/A

in which 6 of 13 spills carried out resulted in RPTs. The up-to-date R&D on this aspect leads to the following observations:[37−39] (a) RPTs at large scales behave differently from their small-scale counterparts; (b) occurrence is significantly influenced by the water temperature and depth of penetration; (c) the strength of RPTs correlates with the spill rate; and (d) RPTs can lead to an increase (up to 65%) in the distance to the LFL. Several theoretical models exist for studying RPTs, such as the superheat theory, the predictive empirical model, and the computational fluid dynamics (CFD) model.[37,38]

3.1.4. Modeling. In recent studies, there have been limited experimental investigations on the formation of LNG pools. Instead, the recent studies seem to be focused more on modeling of this process. Numerical models for LNG pool formation are mainly classified in two categories: the integral model or the Navier−Stokes model. There are numerous models for studying LNG pool formation, including Raj and Kalenkar,[109] Opschoor,[110] SOURCE 5,[41,111−113] GASP,[114,115] SafeSite3G,[116,117] PHAST,[118−122] ALOHA,[123−125] ABS Consulting model,[11] LNGMAP,[11,126,127] and FLACS.[128,129] Of these models, the most commonly used are presented in Table 13.

Integral models originated in the 1980s are the simpler of the two techniques. These models use algebraic equations to obtain solutions and are usually limited to modeling of circular pools, flat substrates, and heat transfer only from the substrates. Examples of some commonly used integral models for pool formation modeling is shown in Table 13. The LNGMAP[11,126,127] seems to be the most robust because of its ability to effectively incorporate real-time geographic information, such as wind effects, current effects, atmospheric conditions, etc., into the model.[126] PHAST[118−122] is an older model than LNGMAP,[11,126,127] seems to be more widely used, and will most likely continue to be because of its ability to model spills on both land and water. PHAST[118−122] is also more superior to SOURCE5[41,111−113] and GASP[114,115] models because of its ability to account for non-circular LNG pool formation and inclusion of heat convection/radiation from sources other than the substrate. Navier−Stokes models are more complex and the most complete models. Modeling pool formation with Navier−Stokes models can be time-consuming because of their complexity. As a result, researchers prefer to model pool formation with integral models and then transfer the data over to Navier−Stokes models for further analysis.[111] A more in-depth description of the Navier−Stokes models is given in section 3.2.4.

The current pool spread models (e.g., the standard model of inertial−gravity spreading) are based on oil pools spreading; however, it is important to note that oil and LNG behave differently.[130] This standard model is applicable for rapidly formed pools; to account for this, many assume that the spill of LNG from a tanker is due to quasi-steady gravity flow.[130] The pressure field is also assumed to be hydrostatic, which is not the case in the pool front. The spread of a LNG pool is treated as inviscid by the standard model, which is a reasonable assumption because of the occurrence of the Liedenfrost effect.[130] Fay[130] carried out studies in which the properties of LNG spills were examined to suggest that a different model should be used and to compare the differences that would ensue from the use of an alternative model.

An alternative model, characterized by an asymptotic spreading law, called the supercritical model was also developed[130] because of questions arising based on the density

ratio between the spill substances and the sea, the effects of the pool leading edge, and the initial and spill conditions. When the maximum radius and evaporation time of the supercritical model were compared to the standard model, a ratio (supercritical to standard) of 2.51 was obtained for the maximum radius and 0.159 for the evaporation time.[130] On the basis of this, a supercritical model would result in a larger maximum radius and shorter evaporation time than the standard model. These findings were also verified by a China Lake experiment,[184] in which the supercritical model had a better fit to experimental data.

3.2. Vapor Dispersion. In the case of unconfined LNG spills on water, the LNG cloud travels at the wind speed prior to dispersion. Because the vapor forms at the boiling temperature of LNG, it will initially be denser than air. For land-based facilities, dense gas behavior is advantageous because it can be easily controlled. However, this can also be a disadvantage because it takes longer to disperse. Most large-scale LNG dispersion tests of spills on water were performed prior to 2007, with the key experimental conditions being summarized in Table 14 by Luketa-Hanlin.[37] The spill volume,

Table 14. LNG Dispersion Test on Water[37]

| experiment	spill volume (m³)	spill rate (m³/min)	pool radius (m)	downwind distance to LFL (m) (maximum)
ESSO	0.73−10.2	18.9	7−14	442
Shell	27−193	2.7−19.3	NA (jettisoned)	2250 (visual)
Maplin Sands	5−20	1.5−4	~10	190 ± 20
Avocet (LLNL)	4.2−4.52	4	6.82−7.22	220
Burro (LLNL)	24−39	11.3−18.4	~5	420
Coyote (LLNL)	8−28	14−19	not reported	310
Falcon (LLNL)	20.6−66.4	8.7−30.3	not reported	380

spill rate, vaporization rate, presence of obstacles, and atmospheric conditions are considered to be key parameters in determining the LFL.[66,68,71] The recent research advance in LNG spill has been focusing on vapor dispersion, including experimental studies on the effect of water curtains, underwater releases, and turbulence on vapor dispersion and modeling studies on the use and development of models for simulating vapor dispersion.

3.2.1. Water Curtains. The water spray curtain is widely used as an inexpensive technique for controlling and mitigating many toxic and flammable vapors. Field tests[131−136] have shown that water curtains can reduce the concentration of LNG vapor clouds and are able to interact with vapor clouds by imparting momentum, heat transfer, and air entrainment. However, the effectiveness of different water curtains (with different flow configurations, drop sizes, coverage heights, and coverage widths) for LNG concentration reduction and temperature increase is still largely unknown. Such knowledge is essential to developing structured engineering guidelines for the design of water curtains in practical applications.

Rana et al.[137,138] investigated the effectiveness of two different water curtains in dispersing LNG vapor cloud using an experimental setup consisting of LNG supplied by a tanker

truck and discharged on a spill area (concrete pad), enclosed with wooden frames. The nozzles selected were 60° full cone spiral and 180° flat-fan water curtain types, which were placed downwind of the spill site. Forced dispersion from the water curtains led to a reduction in the LNG vapor concentration. However, when the strength and dilution ratios of both water curtains were studied, it was evident that the full cone spray is more effective at creating turbulence and, therefore, increasing mixing with air. However, the flat fan is effective in creating a solid barrier and, hence, pushing the vapor cloud upward and reducing the ground level concentration. A further study by Rana et al.[139] involved the LNG been spilled on a water surface. A comparison between the vapor cloud motion from the two studies suggests that water curtains disperse LNG vapor clouds by air entrainment and mixing. From these studies, it is evident that the full cone water curtain is the most efficient (as shown in Figure 6, where the full cone spray resulted in a higher heat
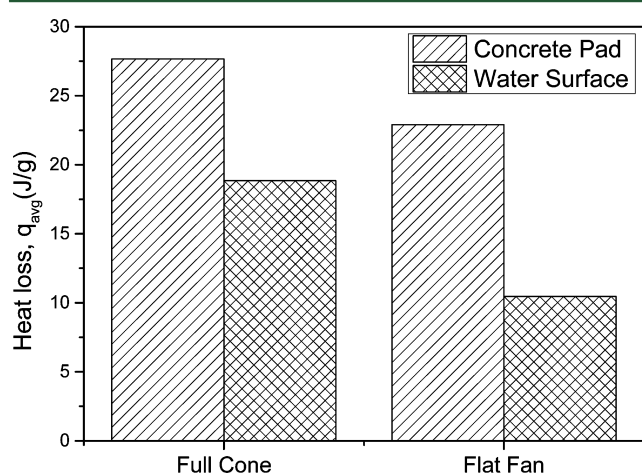
Figure 6. Calculated heat loss by water curtain (data were extracted from the study by Rana et al.[139]).

loss compared to the flat fan). However, a combination of different types of sprays will ensure sufficient mixing, heat transfer, and momentum impact to disperse various size of LNG vapor clouds. Olewski et al.[140] also carried out water curtain dispersion experiments using a smoke trace in place of LNG for safety reasons. A flare was placed in front of an improvised wind tunnel. Two types of flat-fan sprays were tested with several water flow rates and fan speeds, totaling 24 different tests. Experimental results reinforced the findings by other researchers as to the ability of water curtains to control vapor clouds by mechanical- or momentum-transfer effects.

Kim et al.[141] carried out CFD simulation (on a similar experimental setup to that used by Rana et al.[138]) of water curtains using ANSYS Fluent, because current models were not enough to draw a final conclusion on design parameters and the fact that heat transfer and well-defined atmospheric dispersion were not included in most water curtain models. With broadly good prediction, the model simulation overpredicted the experimental data, which was desirable when trying to find the vapor cloud exclusion zone.[141] The added heat-transfer effect was noted to induce a distinct air–vapor mixture, resulting from the natural circulation within the air–vapor mixture. An increase in heat and/or mass transfer lead to a reduction in the vapor cloud exclusion zone. Further CFD simulations by Kim et al.[142] aimed at determining key parameters (including droplet sizes, droplet temperature, and

installation configurations) for water curtain emergency system design. Even though further investigations are required, especially regarding turbulent effects of different sprays, there were several important conclusions: (a) the heat-transfer rate increases with the water flow rate; for droplet sizes ranging from 0.58 to 1.43 mm, a 0.94 mm droplet was noted to have the highest heat-transfer rate per water flow rate; (b) the higher the droplet temperature, the better the dispersion; a 313 K droplet temperature was the most optimal, and any droplet temperature below this showed signs of potential hazards with the LNG vapor cloud flowing around the water curtain because of insufficient heat transfer; and (c) the installation configurations have an optimal tilt angle with the wind (in that case, 60° compared to other angles), and the closer the nozzles are to the source, the better the interaction and forced dispersion of the vapor cloud.

3.2.2. Underwater Releases. Little is known about behavior of LNG following its release underwater, and current models are not sufficient to quantify the potential hazards from such a spill. Using a concrete pit filled with water, Qi et al.[143] carried out tests at the Brayton Fire Training Field to understand the phenomena that occur from an underwater LNG release, including the behavior of the emanating vapor. LNG was released from a 2.5 cm (9.84 in.) nozzle at a depth of 0.71 m (2.33 ft) below the water surface. There was no notable LNG pool formation on the water surface, most likely because of the high rates of evaporation and gas release. It is also possible that all of the LNG was not vaporized underwater but, instead, was thrown up with the rest of the vaporized liquid. The vapor cloud that emanated from the water surface was at a temperature below the dew point of air, and as a result, the vapor cloud was visible. The lowest temperature recorded for the vapor cloud was −1 °C, which explains why the vapor cloud was buoyant because the neutral buoyancy temperature of natural gas is −117 °C.

3.2.3. Effects of Turbulence. The rate of evaporation is necessary for the accurate prediction of the formation, growth, and dispersion of vapor clouds. Typically, it is assumed that the evaporation rate is constant; for example, the detailed CFD study by Cormier et al.[144] used a constant mean evaporation rate. However, it is known that, at the spill point as well as the leading edge of the pool, the turbulence and evaporation rate are both elevated. Morse et al.[145] focused on providing data regarding the evaporation rate of LNG from a water surface by controlling the turbulence. Small-scale experiments were performed in a double-walled vertical cylinder, with a submerged turbulent jet, as shown in Figure 7. The water level was held at a constant level, and once the turbulence surface was established, the LNG was poured onto the water surface. The pressure in the cylinder as well as the temperature of the escaping vapor were recorded and used to calculate the evaporation rate. Morse et al.[145] observed that, for every 1 cm (0.39 in) increase in LNG thickness, there was approximately a 10% increase in the evaporation rate. On the other hand, if turbulence intensity doubles, then the evaporation rate will also double. On the basis of this, it is clear that the evaporation rate depends upon turbulence intensity and, at a smaller level, the thickness of the LNG layer. However, this effect could be different at large scales.

3.2.4. Modeling. Various numerical models have been developed for studying LNG vapor dispersion. The main differences among the models are in the completeness of simulation for the dispersion process, the capabilities in
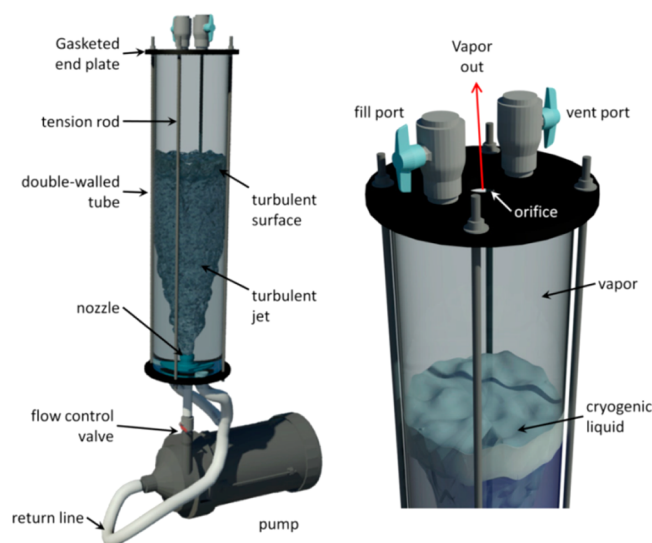
Figure 7. Small-scale experimental setup for measuring the evaporation rate of LNG from a water surface by controlling the turbulence (adapted from the study by Morse and Kytömaa[145]).

different release processes, the ability of the model to describe processes, the completeness in fields and data used, and the complexity of the terrain for which the model is situated.[39] Other differences that are considered when looking at numerical models include the computational requirements, such as power, speed, and memory. Since the 1980s, various numerical models have been developed for the study of atmospheric dispersion of denser than air clouds. Such mathematical models can be classified as either box/top-hat models or Navier−Stokes models.[146]

Box or Top-Hat Models. There are two types of box or top-hat models: modified Gaussian models and similarity-profile models, depending upon the complexity of conservation equations that must be solved.[39] The modified Gaussian models are the simplest because the Gaussian equation is used for the conservation of species while neglecting or simplifying those for momentum and energy.[146] The similarity-profile models use simplified conservation equations with a mathematical complexity of one dimension.[37] Such simplicity is achieved via averaging the LNG cloud properties across the surface of the entire cloud or over the cross wind plane.[37,39] To regain the structural loss because of averaging, similarity profiles are used, therefore leading to quasi-three-dimensional solutions. Examples of similarity-profile models include SCIPUFF,[147] TWODEE,[148,149] SLAB,[150] HEGADAS,[151−153] DEGADIS,[154] ALOHA,[124,125] and GASTAR.[155] Of these models, the most commonly used are SLAB, HEGADAS, DEGADIS, and ALOHA (Table 15).[124,125,150−152,154] ALOHA seems to be the most widely used for safety engineering modeling applications in industry because of its fast computational time and reasonable accuracy.[124] On the other hand, the ease of use and fast computational time of DEGADIS and SLAB have led to them been used in both the public and private sectors.[37]

Navier−Stokes Models. The Navier−Stokes models contain the most physically complete description of the LNG dispersion process and are constructed from three-dimensional and time-dependent conservation equations of momentum, mass, energy, and species.[111,128,129,144,156−160] Examples of Navier−Stokes models that have been used for denser than air modeling include FEM3, FEMSET, FLACS, HEAVYGAS, and

ZEPHYR.[128,129,153,161] Table 16 lists the key features and comparisons of four well-known Navier−Stokes models (FEM3, FLACS, FLUENT, and CFX) for LNG vapor dispersion. It can be seen that, recently, FLUENT and CFX numerical models have been the main Navier−Stokes models used for modeling. This is largely due to the key advantages of these models, including robustness, multiple solving methods, high levels of accuracy, and ability to add to the coding for specific simulations.[162] Although giving a more complete description of the physical processes available and performing better than box or top-hat models,[37] the Navier−Stokes models are more computationally expensive.[146]

The recent developments in modeling are on four aspects, including developments in models, modeling of complex geometries, modeling of complex scenarios (e.g., the effect of wind and ship motion), and evaluation of mathematical models. These advances are summarized below.

3.2.4.1. Developments in Models. The Federal Energy Regulatory Commission (FERC) developed a box/top-hat-type model that uses the model developed by ABS Consulting[11] for source term modeling and DEGADIS for vapor dispersion modeling. The FERC model was successfully used for a comprehensive sensitivity analysis on the effect of tank (25 000 m^3) conditions, release scenarios, and environmental conditions on LNG spill, spread, and dispersion.[163] Table 17 summarizes the main conclusions of the simulations, considering key parameters, such as breach diameter, ullage pressure, weather conditions, and surface roughness, on LNG spill and dispersion.[163] It was concluded that breach size and ullage pressure are important parameters that have a significant effect on LNG spill duration, pool size, and dispersion. LNG spilled from a spherical tank always has a higher spill rate.

The most recent SafeSite$_{3G}$ model is also a box/top-hat-type model that was developed to predict the dynamic effect of LNG discharge and pool ignition on the pool spread process.[116] The model was used for the dynamic analysis of LNG tank (25 000 m^3) release conditions: LNG spreading, dispersion, and combustion. It was found that the bevelled cross-section of a membrane tank can be easily replaced with a rectangular cross-section and still obtain a high degree of accuracy (discharge rate versus time). The analysis showed that, when the average pool depth is above a minimum, both burning and non-burning pools spread at the same rate but the evaporation flux of the discharged LNG is dependent upon turbulence generated during the spill.[116] SafeSite$_{3G}$ was also able to capture and show that, for a period of constant discharge, the discharge rate would be greater than the evaporation rate; this effect was also noted by Johnson et al.[164] using the consequence analysis methodology developed by FERC.

LNGMAP is another box/top-hat-type model that uses a discrete set of algorithms within a geographic information system framework for studying LNG releases and transport in the case of marine spills,[126] overcoming a series of limitations of existing models.[165,166] The model predicts time-dependent release, spreading and transport of LNG on the water surface, LNG evaporation from the water surface (effect of the current and waves), LNG transport and dispersion in the atmosphere, and the burning and associated radiant fields of LNG fires.[126] The model was validated by carrying out simulations presented in the ABS Consulting[11] and Sandia reports.[127] In comparison to the Sandia cases, LNGMAP predicted the distance to the thermal radiation contours being larger for small hole sizes and lower for the largest hole size (see Table 18). LNGMAP was

Table 15. Some Well-Known Similarity-Profile/Modified Gaussian Models for LNG Vapor Dispersion

model	similarity-profile models/modified Gaussian models			
	SLAB[150]	HEGADIS[151−153]	DEGADIS[154]	ALOHA[124,125]
principles	simulates the atmospheric dispersion of denser than air releases	simulates the steady-state or transient ground-level dispersion of a heavy gas cloud	simulates a wide variety of denser than air gas releases	simulates a wide variety of denser than air gas releases
method	spatial averaging to treat the clouds as a steady-state plume, transient puff, or a combination of both Conservation equations of mass, momentum, energy and species	time-dependent model uses a quasi-steady-state description by using "observers"	lumped parameter approach	Gaussian and heavy gas dispersion models
accuracy	LFL was predicted to ±15% for LNG spills	prediction of maximum downwind concentration is overpredicted; however, this prediction then becomes more accurate as the downwind distance increases	downwind gas concentration decay is consistent with experimental data	performed well for all validation tests
validations	Burro and Coyote series tests Eagle series	wind tunnel and laboratory experiments Maplin Sands field tests Thorney Island experiments Goldfish 1 experiment	Burro and Coyote series tests Maplin Sands Thorney Island phase I trials	Prairie Grass Kit Fox
advantages	typical dispersion simulations can be solved in a few minutes on a IBM-AT class computer	simulation of instantaneous releases, time varying releases, and continuous releases	simulation of instantaneous releases, time varying releases, and continuous releases	models puff and plume and heavy gas dispersion simulations can be conducted within a few minutes
disadvantages	cannot model complex terrain or flow around obstacles	cannot model complex terrain or flow around obstacles cannot model elevated source flows	cannot model complex terrain or flow around obstacles	cannot model complex/changing terrain cannot model particulate dispersion
scales	laboratory field	laboratory field	laboratory field	field
applications	ground level evaporating pool, an elevated horizontal jet, a stack or elevated vertical jet, and an instantaneous volume source	dispersion downwind of a transient ground-level source or a vertical transition plane with a near-field jet model heat and water-vapor transfer from substrate gravity slumping and dispersion	prediction of concentrations in the low flammability range	designed for people responding to chemical accidents emergency planning and training
code accessibility	N/A	N/A	N/A	N/A

Table 16. Some Well-Known Navier–Stokes Models for LNG Vapor Dispersion

model	FEM3[157,162]	FLACS[128,129]	FLUENT[111,158,159]	CFX[144,156,160]
		Navier–Stokes models		
principles	initiated in 1973; simulation of large heavier than air gas releases	initiated in the 1980s; simulation of gas dispersion and subsequent explosion	initiated in 1983; simulation of various flow scenarios	simulation of various flow scenarios
method	modified Galerkin finite element method; time-dependent equations of mass, momentum, energy, and species; Reynolds-averaged Navier–Stokes (RANS) equations for calculating the process of momentum; K-theory sub-model for turbulence	finite volume method; time-dependent equations of mass, momentum, energy, and species; k–ε for turbulence	finite volume method; time-dependent equations of mass, momentum, energy, and species; RANS equations and Reynolds stress model (RSM) for calculating the process of momentum; realized k–ε for turbulence; multiple solving approaches	finite volume method; time-dependent equations of mass, momentum, and energy; RANS equations for calculating the process of momentum; k–ε for turbulence; other mathematical models available for modeling processes, such as combustion or radiation; uses a coupled solver
accuracy	underprediction of peak concentration values by a factor of 2; predicts well the salient features in large instantaneous releases	70% of the time, its predicted values are within a factor of 2 of the observed experimental data; can accurately predict down wash from large tanks	RSM predicted the turbulence kinetic energy to within 80% of the expected value, however, reduced to 50% at ground level; gas concentration was within 80% of the experimental data	overprediction of thermal impulses by a factor of 2, however, still acceptable from a safety point of view; underprediction of concentrations at high elevations because of over assumption of gas behavior
validations	Thorney Island phase I trials	Prairie Grass; Kit Fox; EMU; MUST	Burro series field test; DEGADIS model; ADMS model; Falcon tests	Coyote series trials; Brayton Fire Field tests
advantages	3D; can model complex terrain and flow around obstacles; can accommodate multiple instantaneous sources	3D; can model complex terrain and flow around obstacles; distributed porosity concept is used to characterize the geometry while not reducing calculation time as much as other models	3D; can model complex terrain and flow around obstacles; can create user-defined functions; can model temporal and spatial gas dispersion, including gravity slumping and time-dependent effects	3D; can model complex terrain and flow around obstacles; user interface that allows for customization and automation
disadvantages	inappropriate K-theory submodel; cannot model in homogeneous vegetation cover all in the same computational domain; cannot model jet releases, explosive sources, and chemical reactions	in the case of flat terrain simulations, Gaussian models can provide better accuracy than the FLACS model	more complex than other specific models, such as ADMS; long simulation times required	more complex than other specific models; long simulation times required; single solver, unlike FLUENT
scales	field	field; laboratory	field; numerical	field
applications	modeling of gravity slumping and spreading, formation of doughnut-shaped cloud, and cloud bifurcation in the case of LNG spill; submodel for treating aerosol effects in pressurized NH_3 spills; phase-change model for humidity; tool for emergency response planning for liquid CI spills	primarily designed to model explosions in offshore oil platforms; can model dispersion and ventilation in complex geometries	design and optimization of most industrial applications; modeling of complex flows, including turbulence, heat transfer and radiation, chemical reactions, combustion, multiphase flows, and moving geometries	modeling of complex flows, including turbulence, heat transfer and radiation, chemical reactions, combustion, multiphase flows, and moving geometries
code accessibility	N/A	N/A	accessible through user-defined functions	user interface that allows for customization and automation using session files, scripting, and the CFX expression language

Table 17. Effect of the Hole Size and Breach Diameter on Spill and Dispersions Using the FERC Model[a]

parameters	effect of hole size	effect of ullage pressure
time to empty	decreases dramatically with the increase in the hole size; the pool radius also increases (asymptotes at 5 m hole size)	decreases with the increase in the ullage pressure; the pool radius also increases in size
vapor dispersion	decreases dramatically with the increase in the hole size; the pool radius also increases (asymptotes at 5 m hole size)	
LFL		increases with the increase in the ullage pressure (not affect for ullage pressure of >13.79 kPa)

[a]Data were extracted from the study by Qiao et al.[163]

Table 18. Comparison of LNGMAP to Sandia Predictions[a]

	hole size of 1 and 2 m²	hole size of 5 m²
pool diameter (m)	~15–23% larger	~15% lower
spill duration (min)	~1% larger	0% difference
distance to thermal radiation contours (m)	~10–20% larger	10–38% lower

[a]Data were extracted from the study by Spaulding et al.[126]

successfully used to simulate three emergency LNG tanker cases (both with and without ignition of the LNG pool): a tanker continuing on course at 7.5 m/s (24.61 ft/s), a tanker stopping within 3 min, and a tanker changing direction and heading to the nearest location to ground.

Vilchez et al.[167] deviced a "dispersion safety factor" (DSF) based on the concept that, when LNG is spilled on land or water, the visible cloud formed is due to the air reaching the dew point temperature of water, resulting in condensation. DSF can be calculated on the basis of a relationship between the downwind length of the flammable cloud at LFL, X_{LFL} (m), and the downwind length of the visible cloud, X_{VIS} (m): DSF = X_{LFL}/X_{VIS}. With the help of DEGADIS, DSF was validated against the experimental data of Maplin, Burro, and Coyote tests. As humidity increases, DSF decreases, which leads to the flammable region falling within the limits of the visible cloud (safer situation). If humidity decreases, DSF increases, which leads to the flammable region extending beyond the limits of the visible cloud (more dangerous). If X_{VIS} is known, X_{LFL} can be determined via gathering significant sets of data.

3.2.4.2. Modeling of Complex Geometries. Most field studies, with the exception of the Falcon trials, of LNG dispersion are in unobstructed conditions. In practice, in the event of a LNG spill onshore, the receiving terminals are designed to direct the spill toward a sump or impoundment area where a LNG pool is formed.[168] To study the dispersion of natural gas clouds evolving from LNG pools in trenches, Melton et al.[169] deployed a fire dynamics simulator, a CFD model originally developed from modeling thermally driven fluid flow behavior during fires in a 450 000 m³ capacity LNG import terminal. The focus was on the effect of the substrate material and the terrain, via varying the combination of medium-density concrete, spill into trench and flowing to impoundment, and direct spill into impoundment. It was evident that the inclusion of terrain effects increases turbulence and mixing, resulting in shorter dispersion distances (but not always being the case). It is important to define where the LFL is measured from because a "pocket" or isolated volume of cloud can result in a larger LFL, an increase of 10–30% identified in the study.

Gavelli et al.[170] also investigated LNG dispersion from the trench, using a hydraulic model (not accounting for the decrease in the mass flow rate) to analytically calculate the evolving LNG flow and vaporization rate along the trench. This was then imported into CFD FLUENT to calculate the dispersion of the vapors. For cloud dispersion from a trench with perpendicular wind flow direction (relative to the trench), the 1/2LFL extended 65 m (213.25 ft) downwind of the trench and receded before the 10 min spill duration was over as a result of the decreases in heat transfer from the trench. When the wind direction was parallel to the trench, 1/2LFL was in the order of 100 m (328.08 ft). However, the inclusion of a vapor fence had little effect in containing the cloud; instead, it increased turbulence and mixing, increased the dissipation, and decreased the LFL by 30 m.

Considering LNG spill and dispersion into a sump or impoundment, Ponchaut et al.[168] solved the shallow water equations (SWEs). Unlike the integral models, SWEs account for the pool thickness distribution and the growth of the pool with time, using a one-dimensional Fourier conduction equation for modeling the heat transfer. The SWEs account for pool thickness and hydraulic jump, which cannot be modeled by integral models. The pool was predicted to reach the sump wall in 6 s via SWEs, instead of 9 s via PHAST, which is a common integral model. This resulted in a slightly lower vaporization rate in the PHAST model. The effects of elevation of the spill source and the effect of sump floor shape (conical versus flat) were also considered. An increase in the spill source elevation led to a higher peak vaporization rate. However, a conical sump floor would be more favorable in the case of hazard mitigation in cases where the sump floor is close to property boundaries, as peak vaporization was reduced.

3.2.4.3. Modeling of Complex Scenarios. The use of SOURCE5 and DEGADIS is not accurate for predicting flammable vapor dispersion from LNG spills into impoundments because vapor entrainment by wind is not considered. The more accurate CFD package FLUENT was used for such prediction, validated using Falcon test data.[111] The comparison between the CFD simulation results and the experimental data clearly showed that the general shape of the cloud captures the stable stratification that was measured in the experiments. Even though there were some discrepancies, the CFD predictions showed good agreement with the experimental data in terms of the gas concentration profile. The effect of the impoundment and source turbulence were also studied. As expected, the impoundment partially contained the spill and limits its spread in the downwind and lateral directions, while a decrease in source turbulence led to highly stratified and undiluted with vapor cloud within the impoundment. Therefore, mixing seems to be dominated by the turbulence generated by the spill, and the turbulent-driven entrainment affects the rate at which the gas is dispersed and, as a result, the downwind concentrations.

Considering the effect of wind at a −9.3° wind direction, Giannissi et al.[171] simulated the Falcon test series to study the effect of a two-phase jet release, using ADREA-HF, which is a three-dimensional CFD code developed for pollutant and

hazardous gas dispersion studies.[172−174] The simulations considered two cases: the first was a two-phase release, and the second involved a mass flux from the water pond surface, similar to that by Gavelli et al.[111] Both source modeling techniques were in good agreement with the experimental data. However, the two-phase case was better at predicting the maximum concentration and arrival time, and the mass flux case resulted in a longer vapor cloud hold up within the impoundment when compared to the two-phase jet case. This is most likely due to the more realistic/accurate representation of the effect of turbulence generated by the two-phase source as the LNG impacts the water surface. The effect of a −9.3° wind direction was noted to have a large impact on the vapor cloud for the mass flux case, as compared to the two-phase release case. This agrees with the study by Gavelli et al.[111] that, under low wind and stable atmospheric conditions, source turbulence will dominate the mixing and dispersion process. Modeling the spill as a two-phase jet release appears to give a more realistic simulation and more accurate results.

Qi et al.[156] used the CFD code ANSYS CFX to simulate an environmental setup similar to that used in the Falcon series trials, with additional experimental data in the Brayton Fire Training Field (BFTF), where no upwind obstacle was used. It involved spilling LNG into a water surface in an impoundment. The physical behavior of the LNG vapor cloud was well-captured. Unlike the studies conducted by Gavelli et al.[111] and Giannissi et al.,[171] it was clear that both wind velocity and turbulence were dominant in terms of vapor dispersion. This is because, in the experimental work by Qi et al.,[156] the wind velocity was higher and the spill rate was lower (Table 19) than

Table 19. Test Conditions for Spills into Impoundments Followed by Dispersion

	wind speed (m/s)	spill rate (m³/min)
Qi et al.[156]	1.8−2.2	0.265−0.75
Gavelli et al.[111]	1.7	28.7
Giannissi et al.[171]	1.7	28.7

Table 20. Comparison of the Distance to LFL for LNG Dispersion in BFTF[a]

	LFL [5% (v/v) concentration of LNG]	
	at 0.3 m (height)	at 1.22 m (height)
experiment	8.69−13.53 m	6.09−13.47 m
ANSYS CFX simulation	9.80 m	13.47 m

[a]Data were extracted from the study by Qi et al.[156]

that by Gavelli et al.[111] and Giannissi et al.[171] This would result in lower source turbulence, allowing the wind to dominate the flow process. The simulation results from ANSYS CFX were in reasonable overall agreement with the experimental data (as shown in Table 20); however, it underpredicts the ground level gas concentration while underestimating downwind gas concentrations at higher elevations. This suggests that CFX overly assumes the slumping behavior of the gas and takes the buoyancy change less into account. Qi et al.[156] believed that this might be due to an incomplete description of the heat-transfer process during the simulation setup and other sources of uncertainty, such as mesh size and source term turbulence. The cruciality of a sensitivity study in model validation was demonstrated by decreasing the maximum mesh spacing, which

changed the results from underestimated to actually matching the experimental results.

Spaulding et al.[126] found that, in comparison to the stationary case, the moving motion of the vessel leads to much lower concentrations of LNG vapor distributed over a much wider area. This is because, as soon as the vessel stops, the LNG pool will be restricted, reaching a maximum pool area and for a longer duration, therefore resulting in a higher vapor cloud concentration than if it continues moving. A similar conclusion was also deduced for an ignited LNG pool, in which an earlier stop of the vessel results in a more isolated thermal radiated area, which lasts for a longer time. The modular algorithm-based design of LNGMAP makes it able to incorporate new algorithms. Currently, LNGMAP is more computationally efficient than CFD models and, with further advancement, might be confidently used to provide more realistic spill consequences.

There has been little focus on the effect of a substrate temperature to the vaporization of LNG, especially for LNG spills on water. Vesovic[175] investigated the rate of vaporization of LNG, by developing a model for heat transfer from water to the LNG, with the assumption that LNG is released instantaneously and the spreading pool forms a cylindrical shape. The spreading occurs in the gravitational−inertial regime, in which the height of the pool provides the driving force, while the inertia of the ambient water provides the resistance to spreading.[175] Two scenarios were considered: first, the water temperature remains constant, and second, heat arrives to the water surface by conduction only. It was found that the maximum evaporation time is proportional to the fourth root of the initial mass spilled. The derived expression is similar to that by Raj and Kalelkar[109] and Opschoor.[110] However, the results are 10% higher, most likely because of the different assumptions and models used. In the second case, where heat transfer was assumed to be by conduction, the results showed that the rate of vaporization of LNG depends upon not only its composition but also the dynamics and surface temperature of the water. Initially, the thermal inertia of the thin vapor film governs the heat transfer, and 10−15 s after the spill, the transition boiling will start, leading to the thermal inertia of the growing ice layer governing the heat transfer.

3.2.4.4. Evaluation of Models. Various models for simulating LNG dispersion relied on different assumptions and empirical constants, which can cause uncertainty. The uncertainty because of the lack of knowledge (i.e., epistemic uncertainty) can be reduced over time as more data are available, while the uncertainty because of variability within the variables of a model (i.e., aleatory uncertainty) cannot be reduced. Siuta et al.[176] showed that two respective methods can be used to evaluate the uncertainty of models, i.e., the fuzzy sets (FS) theory for analyzing epistemic uncertainty and the Monte Carlo (MC) simulation for analyzing the aleatory uncertainty. These techniques have been successfully applied to evaluate the prediction from the classical model (developed by ABS Consulting),[11] Gaussian dispersion (GD) model, and Britter−McQuaid[177] (BMQ) model for the Maplin Sand and Coyote field experiments (see Table 21).

Ivings et al.[178] proposed a comprehensive model evaluation protocol (MEP) for evaluating the accuracy of various models. The MEP was devised for the NFPA 59A standard. Four main pillars were considered: a model evaluation questionnaire for collecting essential information needed for model assessment, a model validation database with sufficient information for

Table 21. One of the Test Cases Comparing the Addition of the Fuzzy and MC Methods to the Source Term Modeling of the Classical Model[a]

	fuzzy/MC compared to classical model
maximum release rate	~20% lower
spill duration	15% higher
maximum pool radius	12.5–20.7% lower
maximum evaporation time	8.5% lower

[a]Data were extracted from the study by Siuta et al.[176]

verification and validation (following the method developed during the SMEDIS project[179−181]), a set of qualitative and quantitative model assessment criteria (stated in MEP[182]) for qualitative assessment against statistical performance measures, and a comprehensive model evaluation report as key output of the MEP. MEP has been fully used and published for a CFD model by Hansen et al.[183] and for the evaluation of the integral model PHAST that has now been approved for use in LNG siting applications in the U.S.A.

3.3. Combustion. *3.3.1. LNG Pool Fire and Vapor Cloud Fire Experiments.* A variety of LNG fire tests were conducted over the past 3 decades. These fire tests can be classified as fires of LNG pool and vapor cloud on land or fires of LNG pool and vapor on water, with the differences mainly in the burn rate and resulting flame height.[37] In comparison to land LNG pool fires, fires on water have a higher burn rate and flame height by as much as a factor of 2 as a result of additional heat flux from the water.[37] On the other hand, surface emissivity power for both water and land tests has been found to be similar for LNG pool diameters up to 15 m (49.21 ft).[37,40] Table 22 lists the up-to-date large tests for LNG pool and vapor cloud fires, summarized by Luketa-Hanlin[37] and extracted from previous studies.[184−192] It was also found that pool fires are affected by the wind and can be influenced by the shape of any surrounding bunds, whereas surface emissivity is affected by the pool size.[38] The area of burn is also dependent upon the type of ignition.[40]

There has been limited recent research on LNG combustion tests, which focused on the properties/governing factors of pool fires and vapor cloud fires. Lowesmith et al.[193] investigated the nature of two-phased oil and gas jet fires, considering the effects of confinement on jet fires and their behavior with water deluge, for simplifying hazard assessment. Correlations and guidance for assessing jet fires were successfully developed on the basis of experiments from various studies, including those conducted by Advantica Limited, SINTEF, and Shell, since the 1980s.

Studer et al.[194] studied the properties (such as flame visible length, radiation flux, and blowout) of large-scale methane/hydrogen jet fires. The CAST3M code was in good agreement with the experimental results and later used to calculate some safety-related quantities. It was found that, right after ignition, a flame ball formed and the flame length was noted to decrease with time because of a decrease in the mass flow rate. A set of correlations was then developed for estimating the flame length.[194] However, the predictions using these correlations are ~15% lower than those predicted by the correlations developed by Lowesmith et al.,[193] mainly because the released power of the experiments in the study by Studer et al.[194] is at the lower limit of the correlation.

Advances have also been made to develop blowout stability (flame stability) diagrams for different fuels. For example, Wu et al.[195] carried out a study that developed a blowout stability diagram of the hydrogen flame diameter versus atmospheric pressure. Lowesmith et al.[193] developed one for natural gas flames. When the blowout of the Studer et al.[194] experiment was imposed on the flame stability diagrams by Wu et al.[195] and Lowesmith et al.,[193] good agreements were reached. It is clear that the phenomenological model developed by Studer et al.[194] is capable of predicting the flame length, blowout velocities, and radiant fluxes, while Lowesmith et al.[193] presented good background and correlations for jet flame hazard assessment.

3.3.2. Deflagration/Detonation Experiments. Explosion from fuel combustion can be classified as deflagration or detonation. In deflagration, the fuel−air mixture burns slowly at

Table 22. LNG Fire Tests on Water and Land[a]

study	spill terrain	spill volume (m³)	spill rate (m³/min)	pool diameter (m)	flame length (m) (L/D)	surface emissive power (kW/m²)		burn rate, ×10⁻⁴ m/s (kg/m² s)	flame speed for vapor cloud fires (m/s)
						pool fire	vapor cloud fire		
U.S. CG China Lake tests[184−187]	water	3–5.7	1.2–6.6	~15 (effective)	25–55 (2.8–4.4)	210 ± 30 (narrow) 220 ± 50 (wide)	220 ± 30 (narrow) 200 ± 90 (wide)	4–11 (0.18–0.495) (calculated)	8–17 (relative to cloud)
Maplin Sands[189,191]	water	5–20	3.2–5.8	30 (effective)	80 (2.6)	178–248 203 (avg)	137–225 174 (avg)	2.1 (0.0945) (calculated)	4.5–6.0
Coyote[190]	water	14.6–28	13.5–17.1	not measured	not measured	not measured	150–340	not measured	30–50 (near ignition sources)
Maplin Sands[188]	land	not reported	NA	20	43 (2.15)	153 (avg) 219 (max)	NA	2.37 (0.106) (measured)	NA
Montoir[192]	land	238	NA	35	77 (2.2)	290–320 (narrow angle) 257–273 (wide angle) 350 (max)	NA	3.1 (0.14) (measured)	NA

[a]Data were extracted from the study by Luketa-Hanlin[37] that was based on the literature.[184−192]

Table 23. Some Well-Known Models for LNG Fire Modeling

model	point source[196]	solid flame[196−202]	Navier−Stokes[111,160,196]
		LNG fire models	
principles	initiated prior to the 1970s and simulates pool fire as a point at the ground level	initiated prior to the 1970s and simulates fires as a geometric shape, usually on the basis of wind condition	initiated in the 1970s and simulates any type of fire with any shape
method	semi-empirical approach	semi-empirical approach	finite volume method
	inverse square law of radiation	representation of fire as a geometric shape, usually cylinder	time-dependent equations of motion
			$k-\epsilon$ for turbulence
			combustion and soot models can be incorporated
accuracy	provides a reasonably good agreement with experimental data, which is variable because of the assumption made	provides a reasonably good agreement with experimental data, which is variable because of the assumption made	provides good agreement with experimental data if the correct physics is applied
validations	different correlations and related factors have been developed on the basis of findings from experimental work and are selectively used on the basis of the modeling taking place	different correlations and related factors have been developed on the basis of findings from experimental work and are selectively used on the basis of the modeling taking place	via experiments, such as the Esso tests, China Lake tests, Maplin sands tests, Gaz de France, etc.
advantages	simple and can easily produce results	can account for interactions with water vapor and carbon dioxide in the atmosphere	can capture complex flame shapes and interaction of flames with objects
		effects because of wind, such as flame tilt, can be modeled	can model pool fires, vapor cloud fires, and fireballs
disadvantages	energy radiated depends upon a number of factors and is not an intrinsic property of combustion	flames with complex shapes, especially those arising from irregular-shaped pools, cannot be modeled	main disadvantage is the computational requirement compared to other models
	assumes that all radiant energy freed at the ground level	cannot account for flame zones with object interaction	more complex compared to the other models
	assumes that the fire is a small element at the ground level		
	cannot account for wind and obstacle effects		
scales	field	field	field
			laboratory
applications	fire hazard assessment	fire hazard assessment	fire hazard assessment
code accessibility	N/A	N/A	some Navier−Stokes models, e.g., FLUENT and CFX, have accessible codes

speeds in the order of 1 m/s, whereas in detonation, the flame front travels at a shock wave at speeds in the order of 2000–3000 m/s (6561.68–9842.52 ft/s), followed by a combusting wave that supplies it with energy.[37,38] Since the reviews published in 2007, no significant deflagration/detonation experiments have been performed. As concluded previously, detonations are very difficult to achieve in LNG fires because the primary component methane has a low reactivity and deflagrations can transition into a detonation explosion if there is a confinement or blockage.[37,38]

3.3.3. Modeling. A LNG pool fire can transmit significant radiant heat to an object outside the fire, with the heat flux strongly dependent upon various parameters, including the properties of fire (e.g., size, shape, and geometry), surrounding atmosphere (e.g., transmissivity), and object (e.g., location and orientation).[40] Technical issues that arise when modeling LNG pool fires are usually due to the scale of the fire. As pool fires become larger, physical phenomena, such as oxygen starvation in the center of the pool fire, smoke generation, and reduction in the emissivity power, become more important.[38] Extrapolation from small fires can lead to misleading results; therefore, developing modeling techniques are in great need for studying large-scale LNG pool fires.

Typically, there are three approaches to modeling LNG fires: the point source method (simplest), solid flame method (next level of complexity), and field (or Navier–Stokes) method (most complex/complete), as shown in Table 23. The point source model can easily produce results; however, the assumptions taken, such as neglecting wind and obstacle effects, assuming that all heat is radiated at the ground level, can lead to questionable accuracy.[196] On the other hand, the solid flame model accounts for wind and atmospheric condtions; however, the cylindrical flame modeling approach can, at times, lead to inaccurate results.[196−202] Navier–Stokes models as previously discussed in section 3.2.4 are the most complete and robust models that are able to provide the most accurate results.[111,160,196] The same conclusion stated in section 3.2.4 applies here. Fire modeling can only be improved if further evaluation studies are carried. In doing so, issues, such as the effects of radiation, surface emissivity, flame interaction with objects, and pool fire size, need to be studied extensively at the field scale to generate data for model evaluation/validation.

3.3.3.1. Overpressures from LNG Vapor Cloud Ignition. Previous studies for LNG facilities focused on overpressures from ignition of vapor clouds or pool fires from a LNG spill. These analyses were usually performed with simple methods, such as the TNO multi-energy method (MEM) or the Baker–Strehlow–Tang (BST) method.[203] However, these models are inadequate for near-field calculations, are not sensitive to the degree of congestion, and cannot account for obstacles. Gavelli et al.[203] used the advanced modeling tool FLACS to study LNG vapor cloud explosions in two spill scenarios (a worst case and a realistic case) occurring from a 140 000 m³ moss-type LNG vessel moored at an offloading pier. In the worst-case scenario, 23 000 m³ of stoichiometric gas cloud was spilled, and in the realistic scenario (one of many possible encounters), LNG was spilled at the loading rate of 5000 m³/h for 10 s and then dispersed for 3 min by wind. In both cases, the resulting overpressure was well below the minimum threshold for human injury (16.54–20.68 kPa) or facility damage (101.35 kPa).[203] Clearly, the low reactivity of methane results in overpressures, although such overpressures appear to occur within a safe

range, even at an applied safety factor of 2 to account for uncertainties in modeling.

Abe et al.[204] studied the blast effects of the liquid oxygen/LNG fuel mixture using the hypercode ANSYS AUTODYN, considering four cases, including two large-scale liquid fuel explosion of 17 and 5 tonnes, two equivalent scale gas explosions (∼13 and 3.9 tonnes), and 5.8 g of gas explosion. Assumptions, such as wind-free and a steady-state environment, were assumed. From the large-scale simulations, it is clear that overpressures are generated. A secondary shock wave was also noted (believed to be the reflection of the shock wave from the ground). As the overpressure moved further away, the constant volume combustion pressure profile formed is nearly identical to that of a detonation. For the liquid case, blast effects were noted to be 40−50% higher at any distance than those for the gas cases. The properties of the blast wave at relatively long distances were also believed to be independent of ignition conditions. The maximum overpressure recorded was ∼65 kPa [9.42 pounds per square inch gauge (psig)] at 100 m from the explosion point, which is well above the safety thresholds for human (16.54−20.68 kPa) but below that for facilities (101.35 kPa). However, it is important to note that the study did not consider wind disturbances and weather conditions that can have a significant effect on the energy of the overpressure.

3.3.3.2. LNG, LPG, and Gasoline Modeling. The consequence analysis methodology developed by the FERC has become the standard method of modeling LNG release, spread, and pool fires.[164] Vaporization can occur from two mechanisms: heat transfer from the spill surface and heat transfer from a flame. In both cases, FERC methods assume constant heat flux, i.e., 85 kW/m² (0.167 kg m⁻² s⁻¹) for a non-burning LNG pool and 143 kW/m² (0.282 kg m⁻² s⁻¹) for a burning LNG pool. On the other hand, radiation from a flame is modeled by means of the solid flame model.

Johnson and Cornwell[164] performed studies to evaluate the effectiveness of the FERC method in simulating spills, vaporization, and pool fires of material other than LNG (such as LPG and gasoline), considering two release scenarios. In the first scenario of an equal release volume of all three liquids, the burning gasoline pool reached the largest diameter, mainly because of its low vaporization rate, although the impacts from an expanding burning pool were nearly identical for all liquids. In the second scenario of the respective ship containment system of the different liquids, the gasoline pool was still larger than the LNG pool, although the total volume of LNG spilt was 5 times larger. Therefore, LNG release and ignition will not necessarily produce a significantly larger radiant impact than a smaller release of a less volatile material, such as gasoline, for typical cargo containers under similar release conditions. The FERC spill, vaporization, and burning modeling method for LNG can also be used for other material, such as LPG and gasoline, if the correct material properties and physical data are used.

4. SAFETY

Accidental release to the environment poses a risk and requires special care when handling. Marine vessels, unloading facilities, land storage tanks, and processing facilities are considered to be the key areas where risks are to be quantified.[205] The key issues of siting LNG terminals include (a) no exclusion zone siting for spills on water, (b) misleading or erroneous specifications of input parameters for exclusion zone modeling, and (c) the use of unreliable models for exclusion zone calculations.[41] While

Table 24. Comparison of Dosage, Heat Flux, and Duration Needed To Attain First-, Second-, and Third-Degree Burns[206,207,209−212]

	first degree		second degree		third degree	
	dose $[(kW/m^2)^{4/3}\ s]$	heat flux (kW/m^2)	dose $[(kW/m^2)^{4/3}\ s]$	heat flux (kW/m^2)	dose $[(kW/m^2)^{4/3}\ s]$	heat flux (kW/m^2)
Perez et al.[207]	115	0.97−1.63 (60−120 s) 2.73−3.14 (25−30 s)	250	1.73−2.92 (60−120 s) 4.90−5.62 (25−30 s)	421	2.56−4.31 (60−120 s) 7.25−8.32 (25−30 s)
Raj[206]		up to 4 (60−120 s) up to 5 (25−30 s)				
TNO[209]	130	1.06−1.78 (60−120 s) 3.00−3.44 (25−30 s)	390	2.42−4.07 (60−120 s) 6.85−7.85 (25−30 s)	421	2.56−4.31 (60−120 s) 7.25−8.32 (25−30 s)
others[210−212]	118	0.98−1.66 (60−120 s) 2.79−3.2 (25−30 s)	236−239	1.66−2.82 (60−120 s) 4.69−5.44 (25−30 s)		

there have been no major incidents in this industry with the use of the current system, recent studies have focused on safety measures for humans, LNG facilities, and ships, because of rapid increases in production and use of LNG, potential terrorist threats, and public confidence in LNG safety.

4.1. Human. The recent studies regarding human safety focus on thermal hazards from LNG fires rather than the cryogenic effects of a LNG pool/vapor cloud or the asphyxiation from a LNG vapor cloud. Current regulations, such as the U.S. DOT Regulations, 49 CFR, part 193, and the NFPA 59A standard,[173] require that a safety distance is set at a radiant heat flux of 5 kW/m². Unfortunately, there has been no significant research to determine whether this criterion is correct. On the basis of this regulation, Raj[206] conducted some studies on the effectiveness of ordinary civilian clothing to withstand a 30 s exposure of 5 kW/m². It was found that ordinary civilian clothing provides a reduction of radiant heat flux by a factor of 2 and any object that intervenes (even a newspaper held in front of the person) can lead to a reduction by a factor of 4. A person with ordinary civilian clothing can withstand a heat flux of 5 kW/m² for 25−30 s and 4 kW/m² for 60−120 s without severe pain or suffering any injuries. However, repeated exposure without cooling will reduce this tolerance. Raj[206] then concluded that the public should be safe with the current "hazard" definition, which opposes the idea posed by Havens and Spicer[41] that a heat flux of 5 kW/m² will lead to second-degree burns within 30 s. It is important to note that the weather, number of clothing layers, age, sex, and health of people can all play a role in determining the radiant heat flux that can be withstood.

People can easily run from a LNG pool fire, but in the case of a jet fire, flash, or vapor cloud explosion (VCE), the possibility of humans protecting themselves decreases. Probit equations are dimensionless numbers that correlate directly to the percentage of the population affected and considered as a simple and fast method for consequence analysis.[207] VCE produces two damaging properties: pressure waves and thermal effects. The damage because of pressure waves was investigated by Alonso et al.,[208] who uses Probit equations and explosion characteristic curves for human damage consequence analysis, via comparisons between the Probit results and the explosion characteristic curves. Damages, such as eardrum rupture, death because of skull fracture, and lung damage, can then be evaluated and determined for certain distances from the explosion center. This method proposed by Alonso et al.[208] provides a simple and fast consequence analysis that allows for damage to be linked to explosion energy and distance from explosion.

The thermal effects of fires and explosions were studied by Perez et al.,[207] during which new Probit equations were also derived to assist in consequence analysis. Existing Probit equations for thermal effects were devised by TNO[209] in 1989 for first, second, and third degree burns where TNO used assumptions to derived the Probit equation for second degree burns due to insufficient data. Perez et al.[207] derived new Probit equations for calculating thermal dose, benchmarking against the values from TNO and existing literature.[210−212] As shown in Table 24, the Probit equations derived by Perez et al.[207] are in better agreement with the empirical data in the literature than those by TNO. In addition, the results suggest that a heat flux of 5 kW/m² will lead to second-degree burns within 30 s. Such values (0.97−1.63 kW/m² for 60−120 s and 2.73−3.14 kW/m² for 25−30 s) are apparently not in agreement with those (4 kW/m² for 60−120 s and 5 kW/m² for 25−30 s) by Raj.[206] This suggests the need to carry out more experimental testing than can lead to more conclusive results.

4.2. Facilities. In the past, the relatively low demand for natural gas storage made it possible to locate such installations away from densely populated areas. However, it has become clear that there are advantages in bringing storage facilities closer to points of use. When studying the risks involved in a LNG facility, it is therefore crucial to deal with scenarios that are[213] (a) feasible in the course of operation, (b) feasible by interaction with the surroundings, (c) highly improbable but theoretically possible, and (d) intentional damage to the installation with a view of restricting the functions or endangering the surroundings. However, most safety and security documentation barely cover these scenarios. Scenarios a−c can be simulated using typical mathematical models, while for scenario d, modeling of the entrance, including the influence of the protective measure should be taken into account. As a result, Bernatik et al.[213] devised a method adapted from the critical evaluation for national monuments under the National Infrastructure Protection Plan[214] and applied it to a LNG facility. This safety assessment method allows for a simple mathematical equation that considers the type of infrastructure, casualties, economic impact, length of outage, impact on other sectors, and environmental impact that would ensue from a LNG hazard. Coupled with a logical flow process (which involves setting security goals, identifying assets, risks to assets, and implementing protective programs), this method can determine the effectiveness of a protective measure for a LNG facility.

4.2.1. Accident Modeling/Mitigation. Continuous monitoring and implementation of appropriate actions are essential to prevent, control, and mitigate unfavorable consequences of

LNG production and use. LNG facilities have a good safety record, and as a result, failure data on LNG systems are sparse. Because of this limitation in failure data for risk analysis, Yun et al.[215] devised a Bayesian−layer or protection analysis (LOPA) method for obtaining risk with less effort and time compared to most other methods. The Bayesian estimation allows for generic failure data (fire or explosion) from other industries, to be coupled with likelihood information from LNG industry, to determine failure data to be used in the risk analysis. A hazards and operability (HAZOP) study was incorporated, including γ and Poisson distribution for prior and likelihood information. This methodology was validated against existing data and studies to show that it is a powerful method, especially for an industry (such as the LNG industry) where failure data are sparse.

Considering the cryogenic properties and flammable/explosive behavior of LNG, Rathnayaka et al.[216] recently developed and validated a new accident modeling approach that also incorporates a HAZOP based on system safety identification, protection, and prevention (i.e., SHIPP) for applications to a LNG facility. SHIPP is a safety assessment methodology that describes the steps of process safety assessment and provides a guide to possible improvement at every step of the accident process. Following the process accident scenarios identified using HAZOP, the accident process follows three steps: initiation, propagation, and termination. To develop a predictive model for the occurrence of abnormal events, a Poisson probabilistic distribution was incorporated. This method was tested to be reasonably effective using realistic data from a LNG facility,[216] with an over-estimation of up to 14% for the first three time intervals and then underestimations (with decreasing accuracy) as time intervals increase.

On the other hand, Parihar et al.[217] devised a method for consequence analysis at deep-water facilities. The method consists of the use of analytical models to describe the dynamics of unconfined spills, semi-empirical models for pool fires, and CFD for vapor cloud dispersion (this information was previously discussed). Such information is routinely needed for independent risk assessment studies of proposed facilities, and the methodology has been validated and scrutinized against test data.

Li and Huang[218] developed a more mathematical-based approach for assessing the level of risk and damage to facilities and humans at different radii from a LNG fire or explosion. The analysis consists of using the DOW method for fire risk analysis and a VCE model. It is generally accepted that the likelihood of a boiling liquid expanding vapor explosion (BLEVE) occurring in a LNG tank during a LNG pool fire is low because of safety measures currently in place.[219] However, BLEVE should not be disregarded because one BLEVE event did take place in Spain (June 2002), involving a road LNG tanker accident.[220] The BLEVE event is usually followed by a fireball, from which approximately one-fourth of its energy is released as radiation.[221] Li and Huang[218] included BLEVE for risk analysis by making use of the BLEVE model proposed by the International Labour Organization.

In the event of a leakage or emergency, emergency shutdown (ESD) systems in the LNG plants can be used for stopping pumps, etc., and isolating the leakage automatically.[222] Therefore, it is crucial that this ESD system is reliable and always operational to mitigate hazards and prevent escalation. Cheng et al.[223] devised a method in which fault tree analysis

coupled with intuitionistic fuzzy set can be used to assess the reliability and find the component(s) of the ESD that require the most attention. Even though human expertise and knowledge of operations and maintenance of the ESD is required to collect failure information, this method has proven to be able to locate equipment whose improvements will greatly increase the reliability of the ESD and resulting safety of the facility.

Looking from a different perspective, shutdowns are also periods during which maintenance takes place. To prevent the loss of potential revenue during routine shutdowns, Keshavarz et al.[224] determined a risk-based shutdown strategy to minimize the number of shutdowns while maintaining minimal risk for the expected lifetime of the plant. This method is superior to traditional methods because it uses the Weibull distribution rather than linear failure probability methods and can, therefore, accurately and easily use failure history data. The method can be used on both standby and redundant systems and takes into account numerous parameters, including the current costs of the product. It was successfully tested on the PPMR process of APCI, showing that active redundancy reduces the risk for most short goal times. However, as the goal time increases, there is a shift toward the standby strategy for reducing risk, suggesting that standby, active redundancy, and preventative maintenance are crucial to preventing operational risks.[224]

In the case that a pool fire occurs, expansion foam, particularly high-expansion (HEX) foam, can be effective in controlling the LNG pool fire[225] by blanketing the LNG pool surface, as a result preventing oxygen from reaching the fire and also acting as an insulator by reducing fire radiation from the pool fire. A HEX foam application rate of 10 L min^{-1} m^{-2} is the most applicable, and the fire control time can be reduced with an increase in the application rate. The location of foam generation units and design are all crucial factors that should be considered. It is also important that the units are available and operational at all times. Further investigation[226] showed that Foamglas is also able to significantly suppress LNG pool fires and is comparable (if not more effective) to expansion foams. However, Foamglas is not effective at LNG vapor mitigation.

Mitigation is also possible via CFD-based dynamic simulations of hazard consequence reduction. Sun et al.[227] examined both vapor dispersion by water curtains and fire mitigation by HEX foam using CFD validated against the well-known Falcon tests for vapor dispersion and the Montoir tests for pool fire radiation. Water curtains can reduce vapor cloud distance by approximately 61−84%, while HEX foam application leads to a fire control time (time to reduced heat radiation by 90%) of 130 and 55 s, which are comparable to 100 and 60 s from the respective experiments.[225] This clearly demonstrates the great capability and applicability of CFD to hazard mitigation studies.

4.2.2. Other Safety Considerations. The historical safety record of LNG facilities has been excellent, mainly because of the international standard NFPA 59A design codes followed by the designers, constructors, and operators. Taylor[228] presents a summary of the processes (NFPA 59A) that would be followed for site location and equipment placement. On the other hand, Raj and Lemoff[229] discuss the risk evaluation approach of the 2009 edition (latest edition) of the NFPA 59A, compare it to the risk process of Europe, and present an example of how the NFPA 59A can be used. However, the NFPA 59A is still lacking, especially on criteria regarding radiant heat. It is clear

that, with the inclusion of consequence modeling, the process of determining the most cost-effective and safest LNG plant can be accelerated.

Downstream safety in design is for chemical and refinery plants and follows a deterministic approach, while upstream safety in design is for offshore platforms and follows a risk-based approach considering all risks. LNG plants are categorized as midstream safety in design. Because of the increasing number of developments, the modularization concept is being widely applied to onshore LNG plants, leading to the plant design features becoming similar to that of offshore plants. Tanabe and Miyake[230] compare the two approaches and propose a safety design approach for LNG plants, concluding that the most efficient way to ensure the safety integrity of the design is to have a good design basis and minimize uncertainty. Because of less flexibility of the module design, a deterministic approach appears to be more applicable for an onshore modularized LNG plant and the approaches of using a "safety criteria design basis matrix" and a "hazard-design logical relation tree" are effective.[230]

Safety measures that are not usually fully developed at the early stages in current design practices are the emergency systems, the modularized plant and layout, and the tank selection. Because of this, Tanabe and Miyake[231] discuss an approach to enhance safety design application at the concept definition phase. The proposed method is a combination of a "deterministic and risk-based" approach, which can overcome difficulties and restrictions because of limited information at the early stages of a project and will yield schedule and cost benefits.

4.3. Ships. Ships are the major carrier of LNG, and the current world fleet consists of ~400 ships in size of 120 000–250 000 m³.[232] There has been considerable interest in the use of LNG for ship propulsion,[233] such as the dual-fuel steam-turbine mechanical (DFSM) propulsion, dual-fuel gas-turbine electric (DFGE) propulsion, dual-fuel diesel electric (DFDE) propulsion, and diesel mechanical propulsion with reliquefaction (SFDM+R).[234,235] Traditionally, the DFSM propulsion has been the main system used but has a low efficiency,[234] with the increase in LNG carrier size, more suitable propulsion systems, such as the DFGE propulsion system, are required. However, assessment on the applicability, availability, and safety of these systems requires the considerations of numerous factors. For example, in terms of LNG vapor hazards for a gas leak in the DFGE compressor room, CFD simulations (using FLACS) showed that moving gas detectors to within the compressor room will eliminate a 50 s delayed detection time.[234] It was also concluded that there is no benefit in having a second ventilation fan within the compressor room for leaks larger than 1.27 cm, and equipment outside the compressor room will not be affected by any fire that breaks out, unless the equipment is on the roof of the compressor room.[234]

The major contributors of risk associated with LNG shipping can also be determined via high-level risk assessments for LNG carriers. One approach is based on historical data of LNG accidents, published damage statistics, and expert judgments for events, such as collision, grounding, contact, fire and explosion, and other events during loading and unloading.[232] It was found that collision, grounding, and contact were noted together to account for 90% of the total incidents, while LNG containment failure appears be among the highest contributors to risk (Table 25).[232] Therefore, given the good safety record of LNG shipping, it is reasonable to focus more on ensuring that the

Table 25. Distribution of Known Relevant LNG Accidents[232]

accident category	accidents (number)	frequency (per shipyear)
collision	19	6.7×10^{-3}
grounding	8	2.8×10^{-3}
contact	8	2.8×10^{-3}
fire and explosion	10	3.5×10^{-3}
equipment and machinery failure	55	1.9×10^{-2}
heavy weather	9	3.2×10^{-3}
events while loading/unloading	22	7.8×10^{-3}
failure of cargo containment system	27	9.5×10^{-3}
total	158	5.6×10^{-2}

LNG containment systems are designed to an acceptable standard, with cryogenic reliability and high thermal insulation performance for safe and efficient transport of LNG.

4.3.1. Cryogenic Performance of Insulation and Joints. The International Maritime Organisation[236] and the U.S. Coast Guard[237] specify requirements for pressure relief valve sizing on liquefied gas carriers. An example for the adequacy of such requirements is the pressure relief systems to prevent overpressure failure of a current design, polystyrene-foam-insulated, liquid-full moss sphere exposed to a LNG fire. A fire from a 1 m² hole size could have a diameter of more than the length of the ship, could exceed the maximum height of the ship (above the water line), and might burn for 40 min. Havens and Venart[238] conducted a one-dimensional thermal analysis of the moss sphere (steel weather cover > air gap > aluminum foil > polystyrene insulation > aluminum tank wall) using MATLAB for flame temperatures of 1300, 1400, and 1500 K. The failure times of the different parts are shown in Table 26.

**Table 26. Thermal Analysis of the Moss Sphere[a]**

	melting temperature (K)	failure time (s)
steel cover	810	100–180
aluminum foil	873	150–330 after steel cover
polystyrene insulation	510	95–225 after aluminum foil

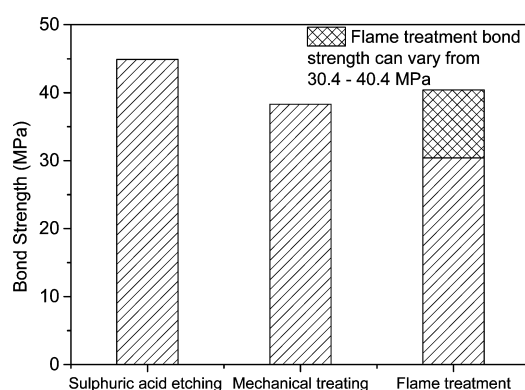[a]Data were extracted from the study by Havens and Venart[238]

At a melting rate of 3 cm/min (1.18 in./min), the polystyrene insulation would be fully melted in less than 10 min. Under such conditions, a moss sphere with non-fire-resistance polystyrene foam protected from a fire by only the steel weather cover could rupture and lead to overpressure if the flames remained for periods longer than 10 min. It was also found that the relief valve equation (by the U.S. Coast Guard) would result in an underprediction of the required relieving capacity by a factor of 9.

The membrane-type LNG tank has two insulation barriers to prevent LNG boil-off and two tightness barriers to protect the hull from low-temperature brittle damage as a result of LNG leaks.[239] The IGC code suggests that the secondary barrier should be designed in a way to contain any LNG spills for at least 15 days.[236] As a result, Bang et al.[239] investigated the cryogenic performance of the adhesively bonded secondary barrier that is composed of an aluminum sheet and a stainless-steel foil (Figure 8) considering the effect of surface treatment, such as mechanical treatment, flame treatment, and sulfuric acid etching on the stainless-steel foil. The sulfuric-acid-etching method showed the highest bond strength (Figure 9), because
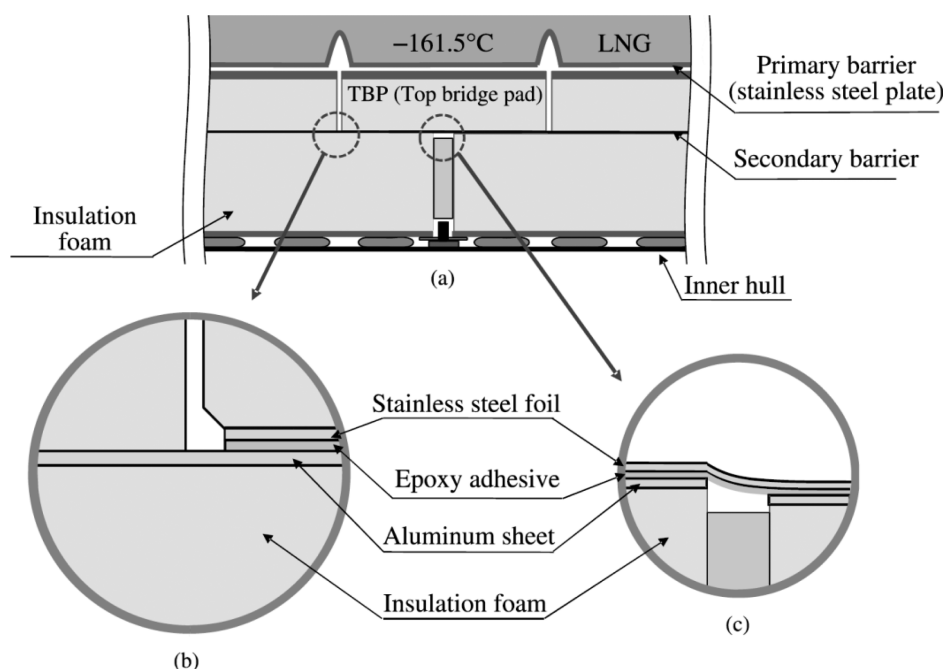
Figure 8. Schematic diagrams of the LNG cargo containment system composed of primary and secondary barriers: (a) overall drawing, (b) enlarged view of the corner of the top bridge pad, and (c) insulation panels with level difference (adapted from the study by Bang et al.[239]).

Figure 9. Effect of the surface treatment on bond strength (data were extracted from the study by Bang et al.[239]).

of nanosize pores that may improve interlocking at the joint. However, the flame treatment method appeared to be the most applicable and productive in the industry, with the application of an optimum treatment time of 5−7 s. After the bonds were subjected to varying thermal-shock loadings, Bang et al.[239] suggested that a 0.15 mm adhesive would be a good control to work from, to create robust adhesive joints for the LNG ship lifetime of 20 years.

Bonding of supporting plates in the primary barrier is usually performed using spot pacing, drilling and tapping, and riveting. Stud welding is a technique that can reduce cost by saving labor and material, but improper processes may cause significant defects and failure of the containment system. Lee et al.[240] carried out numerous experiments to device an optimal stud welding condition for LNG ship containment systems. Via the analyses of bead shape, metallography of the weld, and tensile and bending tests, an optimal condition for stud welds would be a weld current of 520−540 A, a lift of 1.5 mm (gap between the stud bolt and base metal surface), and weld time of 0.4 s, and in the case of a cold weld (because of low fillet height and

incomplete fillet formation), more time and amperage would be required.[240]

Improper bonding or defects from bonding of containment system layers can lead to the formation of cracks and/or leaks. Leakage may also occur if the primary barrier fails and the adhesive joining of the secondary barrier is not thoroughly sealed. Kim et al.[241] investigated the leakage characteristics of composite barriers to devise an improved curing method while limiting residual thermal stresses. It was found that the leakage rate decreases with an increase in the curing temperature and with an increase in the curing pressure from the conventional curing temperature of 25 °C to a high curing temperature of 60 °C. However, increasing the curing temperature also increases residual thermal stresses. An adaptive curing method was created, in which the curing temperature varies based on the solidification of the adhesive, and was shown to decrease the leakage rate by up to 53% without increasing the thermal residual stress, as compared to the conventional 25 °C curing temperature.[241]

Efforts were also taken by other researchers[242] to investigate the crack retardation ability of the composite insulation panel (Figure 8) with glass reinforcement. For efficient transportation, the insulation foam should have very low thermal conductivity for high thermal insulation performance, which limits the density of the foam to less than 120 kg/m^3 [polyurethane foam (PUF)]. Cracks can propagate from this foam because of cyclic thermal loads and low fractural toughness and can lead to failure of the aluminum sheet, resulting in a leak and possibly an explosion. Estimation based on the simulation using finite element software ABAQUS 6.10 and experimental data suggest a maximum strain of 3.5% that would lead to failure of PUF. E-glass fabric (thickness, 0.23 mm; density, 0.25 kg/m^2) was found to be superior as a reinforcement of PUF because it improved the failure strain to 14.3% (over 4 times larger than without the reinforcement).[242]

Yu et al.[243] also investigated the thermal effect of reinforced polyurethane foam (RPUF), including its effect on the

production cost. The insulation foam is limited to a density of less than 120 kg/m³; hence, it is also limited to a glass fiber volume fraction of 0.5% because of thermal properties of the glass fiber. Reinforcing the PUF increases the production cost while decreasing thermal insulation (because of the high thermal conductivity of the glass fiber).[243] Instead of reinforcing PUF with glass fibers of random sizes, Yu et al.[243] compared a normal PUF to RPUF and to others reinforced with single-sized glass fibers of 0.3, 0.7, and 1 mm. As shown in Table 27, selective reinforcement, especially with 1 mm glass fibers, will increase reliability, thermal insulation performance, and manufacturing efficiency at an optimum cost.

Table 27. Tensile Failure Strength and Safety Factor of Insulation Boards with Respect to Different Types of Reinforcements[a]

PUF reinforcement	failure strength (MPa)	safety factor
none	1.8	1.0
0.3 mm glass fibers	4.5	1.4
0.7 mm glass fibers	7.4	1.6
1 mm glass fibers	11.4	2.4
random glass fibers	4.4	1.7

[a]Data were extracted from the study by Yu et al.[243]

4.3.2. Structure. Transportation of LNG is highly dependent upon LNG tanker technology. As discussed in section 2.3, the two mainstream tank systems are the membrane and spherical tank systems (see Table 12), and recently, the membrane tank system has been widely adopted because of its large capacity. The membrane system has a thermal-insulating layer and a metallic membrane covering to maintain liquid tightness without any leakage (as shown in Figure 8). The load of the LNG cargo is transmitted to the thermal insulating layers through the membrane (primary barrier). It is likely that increased sloshing load in large-capacity LNG cargo containers may lead to failure of the corrugated section of the membrane.

Chul Kim et al.[244] employed both experimental methods and finite element analyses (ABAQUS, version 6.7) to evaluate the pressure resistance of the conventional stainless-steel membrane, via applying pressure loads to a 304L stainless-steel corrugated membrane that is in most membrane tanks of Mark-III. Chul Kim et al.[244] found the local yielding and plastic buckling loads of the three types of corrugations (large corrugation, small corrugation, and large corrugation with reinforcing ribs) under the conditions of both symmetric loading and asymmetric loading (Figure 10). The addition of reinforcing ribs only seems to move the stress concentrations toward the ribs and results in larger deformations than the standard corrugations without ribs. Therefore, a new reinforcement method was then developed that inserts 2 mm thick 6061-T6 aluminum pipes into the corrugations. With testing, it was confirmed that this new reinforcement method resulted in no permanent deformation of the corrugations or membrane, as a result increasing the pressure resistance of the membrane without compromising flexibility.

In addition to the membrane with rigid supports (rigid membrane), it is also important to model the membrane with flexible supports in both static and dynamic cases. Finite element analysis (software ABAQUS) for such cases showed that the responses from the dynamic case significantly exceed those of a rigid-supported insulation, demonstrating the need to include both the flexibility and dynamic loading conditions in
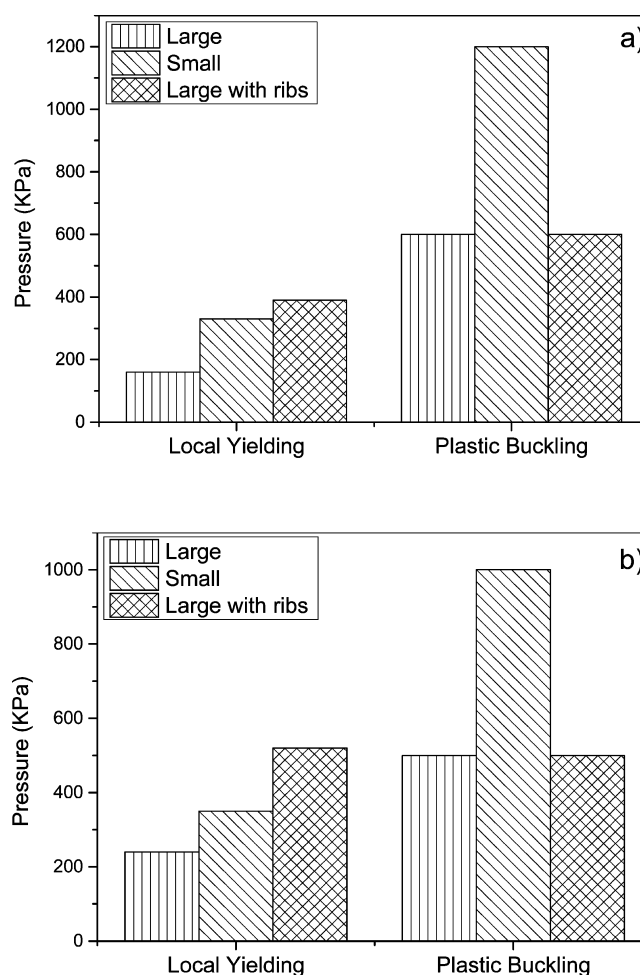
Figure 10. Yielding and buckling pressures of corrugations under symmetric loading: (a) symmetric loading and (b) asymmetric loading (data were extracted from the study by Chul Kim et al.[244]).

analyses for LNG membrane systems.[245] This is particularly important because sloshing flow in ship containment systems is excited by ship motion and the sloshing motion itself can also affect the ship motion. However, up to date, most studies are limited to linear studies of both ship motion and/or sloshing. An example is the study by Pistani and Thiagarajan,[246] in which impact pressures from a sloshing experiment was measured for a two-dimensional tank, with discussion on the problems that would be encountered in sloshing experimentation and how to overcome those problems. Mitra et al.[247] developed an analysis method that coupled both finite difference and time domain panel approaches for three-dimensional sloshing and ship motion capable of predicting both sloshing heights and the hydrodynamic pressures on the containment walls for further analysis. The method was verified against the data from existing scaled experiments. As expected, the sloshing height increases with wave height, and the waves, current, and wind acting at 90° to the direction of the ship motion result in the highest sloshing values. However, the effects of the waves were significantly more dominant (by up to 33%) than that of the wind and currents. The study further illustrates the need to include dynamic effects on studies of sloshing within LNG ship containment systems.

5. FUTURE RESEARCH PERSPECTIVES

With the increasing demand on LNG as an energy source, increasing interest has led to numerous studies regarding the risks involved in LNG production, storage, handling, and transportation. The future research perspectives are briefly summarized below.

5.1. LNG Production. Recent studies regarding the LNG production process focused on the LNG liquefaction and regasification processes, with different configurations proposed and several implemented. Of those that were implemented, optimization was focused on improving efficiency. Future research for maximizing economic profits is required via capital cost reductions to obtain a more complete, economically sound, and efficient LNG plant. In addition, the optimization in the past studies was largely made via the use of a control variable of the regulator control layer, a method of selecting the control variables based on trial and error. Future research is required to develop a self-optimizing complete control structure design for flexibility and economic considerations, although the method requires increasing computational load.

The use of dynamic models for effective control design structures is highly recommended. Variations in design constraints can affect the whole design structure. The use of dynamic models will be especially beneficial for complex processes. In the meantime, further research is needed for the improvement of major equipment, such as multi-stream heat exchangers, drivers, and expanders, and their integration for overall process synthesis and optimization are desired for delivering optimal solutions.

The recent developments include various advances in various aspects of the LNG production process, e.g., the liquefaction processes of improved efficiency. Together with advances in process synthesis and integration, a renewed life cycle analysis of the LNG production process is highly desired to reflect the new advances in the carbon and energy footprints of the fuel.

5.2. LNG Spill, Vapor Production, Dispersion, and Combustion. Despite significant research advances, the dynamics and hazards from a LNG spill require further research. Particularly, there is a lack of experimental data from large-scale spills for determining the possible hazards. Under the circumstances where large-scale experiments are not feasible, specially designed small-scale experiments need to be carried out for validating mathematical models.

Pool Formation. The effect of sea waves on LNG pool formation and spread is not well-understood. A major assumption thus far is that the surface of the sea is flat, while in reality, it is dynamic and turbulent. The effect of currents associated with the waves can also have a large impact on the dynamics of the LNG pool and should be considered in future studies. Future research is also need to investigate the influence of the surface temperature of the substrate on LNG pool formation, especially ice formation from LNG spill on water because of the cryogenic temperatures of the LNG.

Vapor Dispersion. There are various factors affecting LNG vapor clouds, such as the method of release (above water verse under water), spill rate, wind speed, atmospheric stability, RPTs, obstructions, and terrain. Recent studies have added to our knowledge by showing that water curtains are effective methods of controlling LNG vapor dispersion by imparting heat and momentum to the vapor cloud. Any increase in the turbulence of the substrate (spill on water) will lead to an increase in the evaporation rate of the LNG. Obstacles also result in a decreased lower flammability limit, and terrain effects can lead to an increase in turbulence. Therefore, the use of vapor fences for LNG dispersion control can be effective. However, new hazards can develop because of the buildup of vapor within the vapor fence. The past studies were also on small scales; therefore, future experimental investigations are required at medium/intermediate-scale experiments (200 m^3) for reducing epistemic and aleatory uncertainties. In addition, the scientific basis of many models has been questions, especially integral models, so that vapor dispersion simulation using field models (Navier–Stokes models) is highly desired because these models provide the most complete representation of the fundamental fluid dynamics.

Combustion. There have been several studies on LNG fires with the aim of determining the thermal radiation, burn rate, and flame speed. Recent studies have shown that, in the case of LNG vapor cloud ignition, the low reactivity of methane (the main component of LNG) results in overpressures within a safe range, but the likelihood of high overpressures should not be neglected. It is also concluded that LNG releases and ignition will not produce a significantly larger impact than a smaller less volatile material, such as gasoline or LPG. A key gap in the field is the lack of large-scale LNG fire experiments, which should be well-designed and conducted with correct instrumentation in a controlled environment, enabling easier determination of the key parameters affecting the behavior of the flame. As such, more experimental data are essential to the validation of the flame model.

5.3. Safety. The majority of studies on LNG deal with safety to some extent, with some considering the effects of LNG hazards on personal and facilities. Various modeling techniques have been developed for safety assessment of both personnel and LNG facilities, and these techniques may be effective for studying realistic scenarios. Mitigation techniques, such as ESD, routine shutdowns, and the use of HEX and Foamglas, have also been studied, with the aim of improving safety in the most cost-effective way. With regard to LNG carriers, the flame treatment of the aluminum sheets in the insulation barrier of LNG ship containment systems is now known to lead to best bond strength. With the assistance of stud welding of support plates, adaptive curing of the adhesive, and glass reinforced fibers, the insulation foam is believed to provide the best crack retardation ability, leakage prevention, and thermal insulation.

There are at least several aspects that require future R&D. First, it is still unclear whether the current criteria for exposure to a radiant heat flux of 5 kW/m^2 is suitable to prevent second-degree burn injuries. Therefore, further research that also considers the duration of exposure and the physical, thermal, and physiological properties of the receptor need to be conducted to determine whether this radiant heat flux range is suitable. Second, assessments of LNG safety issues need to integrate the credible inputs from the predictions of modeling with relevant complex conditions and geometries tailored to the underlying applications. Third, further improvements are required in the methodology of studying the LNG containment systems of ships. Particularly, the use of dynamic simulations/studies is highly recommended because the effect of dynamic loading (such as sloshing) can exceed those of static-loaded cases.

6. CONCLUDING REMARKS

Significant research advances have been made in the LNG value chain and the understanding and management of the associated risks/safety issues during the handling, storage, and transport of LNG. Recent developments in the LNG production chain were focused on optimizing the process for efficiency improvement, particularly those in the liquefaction and regasification processes, of which several have been implemented. Extensive research has improved our understanding of the fundamental mechanisms that control the dynamics of a LNG spill and the pool formation, vapor dispersion, and potential combustion/fire following such a spill. Such knowledge discovery has allowed for establishing and validating mathematical models for hazard prediction and developing methods for improving the safety of personnel, facilities, and ships. There are still various important technical gaps, and future research is warranted in these important areas for addressing the challenges arising from the rapid increases in production and use of LNG, potential terrorist threats, and public confidence in LNG safety. While there have been no major incidents in the LNG industry with the use of current systems, with further studies and continuous improvements, this safety record can be maintained.

■ AUTHOR INFORMATION

Corresponding Author
*Telephone: +61-8-92667592. Fax: +61-8-92662681. E-mail: h.wu@curtin.edu.au.

Notes
The authors declare no competing financial interest.

■ NOMENCLATURE

avg = average
bcm = billion cubic meters
BFTF = Brayton Fire Training Field
BLEVE = boiling liquid expanding vapor explosion
BOG = boil-off gas
Btu = British thermal units
CFD = computational fluid dynamics
CFR = Code of Federal Regulations
CWHE = coil wound heat exchanger
DFDE = dual-fuel diesel electric
DFGE = dual-fuel gas-turbine electric
DFSM = dual fuel steam-turbine mechanical
DMR = dual mixed refrigerant
DOT = Department of Transportation
DSF = dispersion safety factor
ESD = emergency shutdown
FERC = Federal Energy Regulatory Commission
FLNG = floating liquefied natural gas
FS = fuzzy sets
GA = generic algorithm
GBS = gravity-based structure
HAZOP = hazards and operability
IGC = International Gas Carrier
LFL = low flammability limit
LLNL = Lawrence Livermore National Laboratory
LNG = liquefied natural gas
LOPA = layer of protection analysis
LPG = liquefied petroleum gas
MC = Monte Carlo
MEM = multi-energy method
MEP = model evaluation protocol

MFC = mixed fluid cascade
MM = million
MR = mixed refrigerant
N/A = not applicable or not available
NFPA = National Fire Protection Association
NGL = natural gas liquid
PFHE = parallel fin heat exchanger
PMR = parallel mixed refrigerant
POC = Phillips' optimized cascade
psig = pounds (force) per square inch gauge
PUF = polyurethane foam
RANS = Reynolds-averaged Navier−Stokes
RPT = rapid phase transition
RPUF = reinforced polyurethane foam
RSM = Reynolds stress model
SFDM+R = diesel mechanical propulsion with reliquefaction
SHIPP = system hazard identification, prediction, and prevention
SWE = shallow water equation
tcf = trillion cubic feet
VCE = vapor cloud explosion
X_{LFL} = downwind length to the flammable cloud at the low flammability limit (m)
X_{VIS} = downwind length to the visible cloud (m)
ε = turbulence dissipation rate

■ REFERENCES

(1) British Petroleum (BP). *BP Statistical Review of World Energy 2013*; BP: London, U.K., 2013.

(2) International Energy Agency (IEA). *World Energy Outlook 2012*; IEA: Paris, France, 2012.

(3) United States Energy Information Administration (U.S. EIA). *Annual Energy Outlook 2013—With Projections to 2040*; U.S. EIA: Washington, D.C., 2013.

(4) United States Energy Information Administration (U.S. EIA). *Carbon Dioxide Emissions Coefficients*; U.S. EIA: Washington, D.C., 2013; http://www.eia.gov/environment/emissions/co2_vol_mass.cfm (accessed Nov 2013).

(5) Lim, W.; Choi, K.; Moon, I. *Ind. Eng. Chem. Res.* **2012**, *52*, 3065−3088.

(6) Foss, M. M. *Introduction to LNG*; Center for Energy Economics, Bureau of Economic Geology, The University of Texas at Austin: Austin, TX, 2003.

(7) Starling, K. E.; Savidge, J. L. *Compressibility Factors of Natural Gas and Other Related Hydrocarbon Gases*; Operating Section, American Gas Association: Washington, D.C., 1992.

(8) Shaw, B.; Shaw, G. *Liquefied Petroleum Gas (LPG), Liquefied Natural Gas (LNG) and Compressed Natural Gas (CNG)*; http://www.envocare.co.uk/lpg_lng_cng.htm (accessed Nov 2013).

(9) Katz, D. L. *Handbook of Natural Gas Engineering*; McGraw-Hill Book Company, Inc.: New York, 1959.

(10) National Institute of Standards and Technology (NIST). *NIST Chemistry WebBook*; NIST: Gaithersburg, MD, 2011; http://webbook.nist.gov/chemistry/ (accessed Nov 2013).

(11) ABS Consulting, Inc. *Consequence Assessment Methods for Incidents Involving Releases from Liquefied Natural Gas Carriers*; ABS Consulting, Inc.: Houston, TX, 2004; p 128.

(12) Murdock, J. W. *Fundamental Fluid Mechanics for the Practicing Engineer*, 1st ed.; CRC Press: Boca Raton, FL, 1993.

(13) Wegrzyn, J.; Powars, C. *Best Practices To Avoid Liquefied Natural Gas Fueling Station Venting Losses*; Brookhaven National Laboratory: Washington, D.C., 2012.

(14) Howell, J.; Harger, J. *CNC and LNG: What's Best for Your Fleet*; Westport: New York, 2013.

(15) Wood, D. A. *J. Nat. Gas Sci. Eng.* **2012**, *9*, 16−27.

(16) United States Energy Information Administration (U.S. EIA). *International Energy Outlook 2013*; U.S. EIA: Washington, D.C., 2013.

(17) Western Australian State Government. *LNG Industry Profile—Strategic Policy*; Department of State Development, Western Australian State Government: Perth, Western Australia, Australia, 2012; p 5.

(18) Boskalis. *The Brass LNG Project (Nigeria)*; Boskalis: Papendrecht, Netherlands, 2013.

(19) Castillo, L.; Nadales, R.; Gonzalez, C.; Dorao, C. A.; Viloria, A., Technology selection for liquefied natural gas (LNG) on baseload plants. *Proceedings of the XIX International Gas Convention*; Caracas, Venezuela, May 24−26, 2010.

(20) Humphrey, G. *Current State and Outlook for the LNG Industry*; http://www.forum.rice.edu/wp-content/uploads/2011/06/RT_110909_Humphries.pdf (accessed Nov 2013).

(21) United States Energy Information Administration (U.S. EIA). *Algeria Overview*; U.S. EIA: Washington, D.C., 2013; p 16.

(22) Prasetyo, N. H. *Maintaining Excellence in a Declining Production*; Process and SHE Engineering, PT Badak NGL: Bontang, Indonesia, 2013.

(23) Ukpohor, E. T. O. Nigerian gas masster plan: Strenthening the nigeria gas infrastructure blueprint as a base for expanding regional gas market. *Proceedings of the 24th World Gas Conference*; Buenos Aires, Argentina, Oct 5−9, 2009.

(24) Qatargas. *Inovation in Global Energy*; Qatargas Operating Company, Ltd.: Qatar, 2012.

(25) Total. *Yamal LNG: Harnessing the Arctic's Gas Resources*; http://total.com/en/energies-expertise/oil-gas/exploration-production/projects-achievements/lng/yamal-lng (accessed Nov 2013).

(26) Okamura, T.; Furukawa, M.; Ishitani, H. *Appl. Energy* **2007**, *84*, 1136−1149.

(27) Foss, M. M. *An Overview on Liquefied Natural Gas (LNG), Its Properties, the LNG Industry, and Safety Considerations*; The University of Texas at Austin: Austin, TX, 2012.

(28) Tusiani, M.; Shearer, G. *LNG: A Nontechnical Guide*; PennWell Corp.: Tulsa, OK, 2007; p 436.

(29) United States Energy Information Administration (U.S. EIA). *The Global Liquefied Natural Gas Market: Status and Outlook*; U.S. EIA: Washington, D.C., 2003.

(30) Barnett, P. J. Life cycle assessment (LCA) of liquefied natural gas (LNG) and its environmental impact as a low carbon energy source. B.Eng. Research Thesis, University of Southern Queensland, Toowoomba, Queensland, Australia, 2010.

(31) Burnham, A.; Han, J.; Clark, C. E.; Wang, M.; Dunn, J. B.; Palou-Rivera, I. *Environ. Sci. Technol.* **2011**, *46*, 619−627.

(32) Lavray, H. *Life Cycle Assessment of Electricity Generation*; Eurelectric: Brussels, Belgium, 2011.

(33) Cherubini, F.; Bird, N. D.; Cowie, A.; Jungmeier, G.; Schlamadinger, B.; Woess-Gallasch, S. *Resour., Conserv. Recycl.* **2009**, *53*, 434−447.

(34) Ou, X.; Zhang, X.; Chang, S.; Guo, Q. *Appl. Energy* **2009**, *86*, 197−208.

(35) Jaramillo, P.; Griffin, W. M.; Matthews, H. S. *Environ. Sci. Technol.* **2007**, *41*, 6290−6296.

(36) Bridgwood, P. *Improved LNG Process*; Liquefied Natural Gas, Ltd.: Perth, Western Australia, Australia, 2013.

(37) Luketa-Hanlin, A. *J. Hazard. Mater.* **2006**, *132*, 119−140.

(38) Cleaver, P.; Johnson, M.; Ho, B. *J. Hazard. Mater.* **2007**, *140*, 429−38.

(39) Koopman, R. P.; Ermak, D. L. *J. Hazard. Mater.* **2007**, *140*, 412−28.

(40) Raj, P. K. *J. Hazard. Mater.* **2007**, *140*, 444−464.

(41) Havens, J.; Spicer, T. *J. Hazard. Mater.* **2007**, *140*, 439−43.

(42) Natural Gas Supply Association (NGSA). *Natural Gas—Background*; http://naturalgas.org/overview/background/ (accessed Nov 2013).

(43) Cook, P. P.; Beck, D. V.; Brereton, P. D.; Clark, P. R.; Fisher, D. B.; Kentish, P. S.; Toomey, M. J.; Williams, D. J. *Engineering Energy: Unconventionl Gas Production*; Australian Council of Learned Academies (ACOLA): Melbourne, Victoria, Australia, 2013.

(44) Al-shobi, S. A. Simulation and integration of liquefied natural gas (LNG) processes. M.Sci. Thesis, Texas A&M University, College Station, TX, 2007.

(45) Poten & Partners and Merlin Associates. *LNG Cost and Competition*, 2 ed.; Poten & Partners and Merlin Associates: New York, 2004.

(46) Arrow LNG. *Environmental Impact Statement*; Arrow Energy: Brisbane Queensland, Australia, 2012.

(47) Mokhatab, S.; Economides, M. J. Onshore LNG production process selection. *Proceedings of the SPE Annual Technical Conference and Exhibition*; San Antonio, TX, Sept 24−27, 2006.

(48) Marin. *Report—A Newsletter of MARIN*; Marin: Wageningen, Netherlands, 2003; Vol. *81*, pp 1−19.

(49) Andress, D. L. *The Phillips Optimized Cascade LNG Process: A Quarter Century of Improvements*; Phillips Petroleum Company: Bartlesville, OK, 1996.

(50) Martin, P. Y.; Fischer, B. Natural gas liquefaction processes comparison. *Proceedings of the 14th International Conference and Exhibition on Liquefied Natural Gas*; Doha, Qatar, 2004.

(51) Shukri, T. *Hydrocarbon Eng.* **2004**, *9*, 71−76.

(52) ConocoPhillips. *Optimized Cascade Process*; http://lnglicensing.conocophillips.com/EN/Documents/ConocoPhillipsLNG_Brochure.pdf (accessed Nov 2013).

(53) Michelsen, F. A.; Lund, B. F.; Halvorsen, I. J. *Ind. Eng. Chem. Res.* **2010**, *49*, 8624−8632.

(54) Stebbing, R.; O'Brien, J. *An Updated Report on the PRICO Process for LNG Plant*; LNG & LPG Technology Congress: Paris, France, 1975; GASTECH 75.

(55) Singh, A.; Hovd, M. Dynamic modeling and control of the PRICO LNG process. *Proceedings of the AIChE Annual Meeting*; San Francisco, CA, March 30−April 3, 2006.

(56) Swenson, L. K. Single mixed refrigerant, closed loop process for liquefying natural gas. U.S. Patent 4,033,735, 1977.

(57) Schmidt, W.; Kennington, B. *LNG J.* **2011**, 8−12.

(58) McKeever, J.; Pillarella, M.; Bower, R. *LNG Ind.* **2008**, 44−49.

(59) Pillarella, M.; Liu, Y.-N.; Petrowski, J.; Bower, R. The C3MR liquefaction cycle: Versatility for a fast growing, ever changing LNG industry. *Proceedings of the 15th International Conference and Exhibition on Liquefied Natural Gas*; Barcelona, Spain, April 24−27, 2007.

(60) Longsworth, R. C. Cryostat with serviceable refrigerator. U.S. Patent 4,277,949, 1981.

(61) Liu, Y.-N.; Newton, C. L. Feed gas drier precooling in mixed refrigerant natural gas liquefaction processes. U.S. Patent 4,755,200, 1988.

(62) Martin, P.-Y.; Pigourier, J.; Fischer, B. *Hydrocarbon Eng.* **2004**, *9*, 75−79.

(63) Dam, W.; Ho, S.-M. *Oil Gas J.* **2001**, *99*, 58−58.

(64) Newton, C. L. Dual mixed refrigerant natural gas liquefaction with staged compression. U.S. Patent 4,525,185, 1985.

(65) van de Graaf, J. M.; Pek, B. *Large-Capacity LNG Trains: The Shell Parallel Mixed Refrigerant Process*; LNG and Gas Processing Group, Shell Global Solutions International BV: The Hague, Netherlands, Oct 2005.

(66) Flesch, E.; Raillard, J.-C.; de France, G. CII liquefaction process: 2 cascades into 1. *Proceedings of the 12th International Conference and Exhibition on Liquefied Natural Gas*; Perth, Western Australia, Australia, (May 4−7, 1998; pp 4−7.

(67) Roberts, M. J.; Agrawal, R. Hybrid cycle for the production of liquefied natural gas. U.S. Patent 6,308,531, 2001.

(68) Roberts, M.; Liu, Y.; Bronfenbrenner, J.; Petrowski, J. Reducing LNG capital cost in today's competitive environment. *Proceedings of the 14th International Conference and Exhibition on Liquefied Natural Gas*; Doha, Qatar, March 21−24, 2004.

(69) Bauer, H. A novel concept for large LNG baseload plants, *Proceedings of the 2001 AIChE Spring National Meeting*; Houston, TX, April 22−26, 2001.

(70) Berger, E.; Forg, W.; Heiersted, R.; Paurola, P. *The MFC (Mixed Fluid Cascade) Process for the First European Baseload LNG Production Plant*; Linde Technology: Munich, Germany, 2003; p 12.

(71) Barron, R. F. *Cryogenic Systems*; Oxford University Press: New York, 1985.

(72) Walker, G. *Cryocoolers*; Plenum Press: New York, 1983; p 392.

(73) Timmerhaus, K. D.; Flynn, T. M. *Cryogenic Process Engineering*; Plenum Press: New York, 1989.

(74) Alabdulkarem, A.; Mortazavi, A.; Hwang, Y.; Radermacher, R.; Rogers, P. *Appl. Therm. Eng.* **2011**, *31*, 1091−1098.

(75) Paradowski, H.; Bamba, M.; Bladanet, C. Propane precooling cycles for increased LNG train capacity. *Proceedings of the 14th International Conference and Exhibition on Liquefied Natural Gas*; Doha, Qatar, March 21−24, 2004; pp 107−124.

(76) Venkatarathnam, G. *Cryogenic Mixed Refrigerant Processes*; Springer: New York, 2008.

(77) Khan, M. S.; Lee, S.; Rangaiah, G. P.; Lee, M. *Appl. Energy* **2013**, *111*, 1018−1031.

(78) Castillo, L.; Majzoub Dahouk, M.; Di Scipio, S.; Dorao, C. A. *Energy Convers. Manage.* **2013**, *66*, 41−47.

(79) Baek, S.; Hwang, G.; Lee, C.; Jeong, S.; Choi, D. *Energy Convers. Manage.* **2011**, *52*, 2807−2814.

(80) Lim, W.; Lee, I.; Tak, K.; Cho, J. H.; Ko, D.; Moon, I. *Ind. Eng. Chem. Res.* **2014**, *53*, 1973−1985.

(81) Rodgers, P.; Mortazavi, A.; Eveloy, V.; Al-Hashimi, S.; Hwang, Y.; Radermacher, R. *Appl. Therm. Eng.* **2012**, *48*, 41−53.

(82) Wahl, P. E.; Løvseth, S. W.; Mølnvik, M. J. *Comput. Chem. Eng.* **2013**, *56*, 27−36.

(83) Wang, M.; Zhang, J.; Xu, Q. *Comput. Chem. Eng.* **2012**, *39*, 84−95.

(84) Chang, H.-M.; Lim, H. S.; Choe, K. H. *Cryogenics* **2012**, *52*, 642−647.

(85) Rian, A. B.; Ertesvåg, I. S. *Energy Fuels* **2012**, *26*, 1259−1267.

(86) Li, Y.; Wang, X.; Ding, Y. *Appl. Energy* **2012**, *99*, 484−490.

(87) Li, Q. Y.; Ju, Y. L. *Appl. Therm. Eng.* **2010**, *30*, 2518−2525.

(88) Lukaszewski, M. W.; Zimmerman, W. B. J.; Tennant, M. T.; Webster, M. B. *Chem. Eng. Res. Des.* **2013**, *91*, 457−463.

(89) MAN Diesel & Turbo. *Propulsion Trends in LNG Carriers*; MAN Diesel & Turbo: Copenhagen, Denmark, 2009.

(90) Woehrling, J.-M.; Cotterell, C. D. *International Safety Guide for Inland Navigation Tank-barges and Terminals (ISGINTT)*; Central Commission for the Navigation of the Rhine: Strasbourg, France, 2010.

(91) Peebles, M. W. H. *Natural Gas Fundamentals*; Shell International Gas Limited: The Hague, Netherlands, 1992.

(92) Rudan, S.; Ascic, B.; Visic, I. *Proceedings of the 6th International Conference on Collision and Grounding of Ship and Offshore Structures*; Trondheim, Norway, June 17−19, 2013; pp 331−337.

(93) Querol, E.; Gonzalez-Regueral, B.; García-Torrent, J.; Ramos, A. *Appl. Energy* **2011**, *88*, 2382−2390.

(94) Liu, C.; Zhang, J.; Xu, Q.; Gossage, J. L. *Ind. Eng. Chem. Res.* **2010**, *49*, 7412−7420.

(95) Tsatsaronis, G.; Morosuk, T. *Energy* **2010**, *35*, 820−829.

(96) Morosuk, T.; Tsatsaronis, G. *Energy* **2011**, *36*, 3771−3778.

(97) Morosuk, T.; Tsatsaronis, G.; Boyano, A.; Gantiva, C. *Int. J. Energy Environ. Eng.* **2012**, *3*, 1−9.

(98) Dispenza, C.; Dispenza, G.; La Rocca, V.; Panno, G. *Appl. Therm. Eng.* **2009**, *29*, 380−387.

(99) Dispenza, C.; Dispenza, G.; Rocca, V. L.; Panno, G. *Appl. Therm. Eng.* **2009**, *29*, 388−399.

(100) Shi, X.; Che, D. *Energy Convers. Manage.* **2009**, *50*, 567−575.

(101) Liu, Y.; Guo, K. *Energy* **2011**, *36*, 2828−2833.

(102) Zhang, N.; Lior, N. *Energy* **2006**, *31*, 1666−1679.

(103) Dispenza, C.; Dispenza, G.; Rocca, V. L.; Panno, G. *Appl. Therm. Eng.* **2009**, *29*, 3595−3608.

(104) La Rocca, V. *Energy* **2010**, *35*, 2049−2058.

(105) La Rocca, V. *Energy* **2011**, *36*, 4897−4908.

(106) Messineo, A.; Panno, G. *J. Nat. Gas Sci. Eng.* **2011**, *3*, 356−363.

(107) Koopman, R. P.; Baker, J.; Cederwall, R. T.; Goldwire, H. C. J.; Hogan, W. J.; Kamppinen, L. M.; Kiefer, R. D.; McClure, J. W.; McRae, T. G.; Morgan, D. L. *LLNL/NWC 1980 LNG Spill Tests. Burro Series Data Report*; Lawrence Livermore National Laboratory (LLNL): Livermore, CA, 1982; p 290.

(108) Conrado, C.; Vesovic, V. *Chem. Eng. Sci.* **2000**, *55*, 4549−4562.

(109) Little, D.; Raj, P. P.; Guard, U. S. C. *Assessment Models in Support of the Hazard Assessment Handbook*; Arthur D. Little, Inc.: Cambridge, MA, 1974.

(110) Opschoor, G. *Cryogenics* **1977**, *17*, 629−634.

(111) Gavelli, F.; Bullister, E.; Kytomaa, H. *J. Hazard. Mater.* **2008**, *159*, 158−168.

(112) Atallah, S.; Sirdesai, M.; Jennings, D. M. *Source1: A Model for Creating a DEGADIS Input File*; Gas Research Institute (GRI): Des Plaines, IL, 1993.

(113) Raj, P. K.; O'Farrel, P. M. *Development of Additional Hazard Assessment Models*; Arthur D. Little, Inc.: Cambridge, MA, 1977.

(114) Webber, D. M.; Jones, S. J. A model of spreading vaporising pools. In *International Conference on Vapour Cloud Modelling*; Woodward, J., Ed.; American Institute of Chemical Engineers (AIChE): New York, 1987.

(115) Netherlands Organisation for Applied Scientific Research (TNO). *Methods for the Calculation of Physical Effects (TNO Yellow Book)*; TNO: The Hague, Netherlands, 1997.

(116) Woodward, J. L. *J. Hazard. Mater.* **2007**, *140*, 478−487.

(117) Woodward, J. L.; Pierorazio, A. J. SS3G—An integrated risk analysis program using engineering principles for building damage. *Proceedings of the Mary Kay O'Connor 2001 Annual Symposium*; College Station, TX, Oct 30−31, 2001; pp 365−382.

(118) Witlox, H. W. M.; Oke, A. *Verification and Validation of Consequence and Risk Models for Accidental Releases of Hazardous Chemicals to the Atmosphere*; DNV Software: London, U.K., 2007.

(119) McQuaid, J. *Some Experiments on the Structure of Stable-Stratified Shear Flows*; Safety in Mines Research Establishment, Health and Safety Executive: Liverpool, U.K., 1976.

(120) Petersen, R. L. *J. Wind Eng. Ind. Aerodyn.* **1990**, *36*, 643−652.

(121) Pitblado, R.; Baik, J.; Hughes, G.; Ferro, C.; Shaw, S. *Process Saf. Prog.* **2004**, *24*, 108−114.

(122) Pitblado, R.; Baik, J.; Raghunathan, V. *J. Hazard. Mater.* **2006**, 148−154.

(123) Thoman, D. C.; O'Kula, K. R.; Laul, J. C.; Davis, M. W.; Knecht, K. D. *J. Chem. Health Saf.* **2006**, *13*, 20−33.

(124) Bernatik, A.; Libisova, M. *J. Loss Prev. Process Ind.* **2004**, *17*, 271−278.

(125) Mazzoldi, A.; Hill, T.; Colls, J. J. *Atmos. Environ.* **2008**, *42*, 8046−8054.

(126) Spaulding, M. L.; Swanson, J. C.; Jayko, K.; Whittier, N. *J. Hazard. Mater.* **2007**, *140*, 488−503.

(127) Hightower, M.; Gritzo, L.; Luketa-Hanlin, A.; Covan, J.; Tieszen, S.; Wellman, G.; Irwin, M.; Kaneshige, M.; Melof, B.; Morrow, C.; Ragland, D. *Guidance on Risk Analysis and Safety Implications of a Large Liquefied Natural Gas (LNG) Spill over Water*; Sandia National Laboratories: Albuquerque, NM, 2004; p 168.

(128) Dharmavaram, S. *Process Saf. Prog.* **2005**, *24*, 316−272.

(129) Hanna, S. R.; Hansen, O. R.; Dharmavaram, S. *Atmos. Environ.* **2004**, *38*, 4675−4687.

(130) Fay, J. A. *J. Hazard. Mater.* **2007**, *140*, 541−51.

(131) Dandrieux, A.; Dusserre, G.; Thomas, O. *Environ. Modell. Software* **2003**, *18*, 253−259.

(132) Hald, K.; Buchlin, J.-M.; Dandrieux, A.; Dusserre, G. *J. Loss Prev. Process Ind.* **2005**, *18*, 506−511.

(133) McQuaid, J.; Fitzpatrick, R. D. *J. Occup. Accid.* **1983**, *5*, 121−133.

(134) McQuaid, J.; Fitzpatrick, R. D. *The Uses and Limitations of Water-Spray Barriers*; Health and Safety Executive: Liverpool, U.K., 1981.

(135) Moodie, K. *Plant/Oper. Prog.* **1985**, *4*, 234−241.

(136) Moore, P. A. C.; Rees, W. D. *Forced Dispersion of Gases by Water and Steam*; North Western Branch Papers, Institution of Chemical Engineers (IChemE): London, U.K., 1981.

(137) Rana, M. A.; Cormier, B. R.; Suardin, J. A.; Zhang, Y.; Mannan, M. S. *Process Saf. Prog.* **2008**, *27*, 345−353.

(138) Rana, M. A.; Guo, Y.; Mannan, M. S. *J. Loss Prev. Process Ind.* **2010**, *23*, 77−88.

(139) Rana, M. A.; Mannan, M. S. *J. Loss Prev. Process Ind.* **2010**, *23*, 768−772.

(140) Olewski, T.; Nayak, S.; Basha, O.; Waldram, S.; Véchot, L. *J. Loss Prev. Process Ind.* **2011**, *24*, 798−804.

(141) Kim, B. K.; Ng, D.; Mentzer, R. A.; Mannan, M. S. *Ind. Eng. Chem. Res.* **2012**, *51*, 13803−13814.

(142) Kim, B. K.; Ng, D.; Mentzer, R. A.; Mannan, M. S. *J. Loss Prev. Process Ind.* **2013**, *26*, 1670−1678.

(143) Qi, R.; Raj, P. K.; Mannan, M. S. *J. Loss Prev. Process Ind.* **2011**, *24*, 440−448.

(144) Cormier, B. R.; Qi, R.; Yun, G.; Zhang, Y.; Mannan, M. S. *J. Loss Prev. Process Ind.* **2009**, *22*, 332−352.

(145) Morse, T. L.; Kytömaa, H. K. *J. Loss Prev. Process Ind.* **2011**, *24*, 791−797.

(146) Ermak, D. L.; Rodean, H. C.; Lange, R.; Chan, S. T. *A Survey of Denser-than-Air Atmospheric Dispersion Models*; Lawrence Livermore National Laboratory (LLNL): Livermore, CA, 1988.

(147) Sykes, R. I.; Cerasoli, C. P.; Henn, D. S. *J. Hazard. Mater.* **1999**, *64*, 223−247.

(148) Hankin, R. K.; Britter, R. E. *J. Hazard. Mater.* **1999**, *66*, 211−226.

(149) Hankin, R. K. S. *J. Hazard. Mater.* **2003**, *103*, 1−10.

(150) Ermak, D. L. *User's Manual for SLAB: An Atmospheric Dispersion Model for Denser-than-Air Releases*; Lawrence Livermore National Laboratory (LLNL): Livermore, CA, 1990.

(151) Witlox, H. W. M. *Atmos. Environ.* **1994**, *28*, 2917−2932.

(152) Witlox, H. W. M. *Atmos. Environ.* **1994**, *28*, 2933−2946.

(153) Blackmore, D. R.; Herman, M. N.; Woodward, J. L. *J. Hazard. Mater.* **1982**, *6*, 107−128.

(154) Spicer, T. O.; Havens, J. A. *J. Hazard. Mater.* **1987**, *16*, 231−245.

(155) Hanna, S. R.; Chang, J. C.; Strimaitis, D. G. *Atmos. Environ., Part A* **1993**, *27*, 2265−2285.

(156) Qi, R.; Ng, D.; Cormier, B. R.; Mannan, M. S. *J. Hazard. Mater.* **2010**, *183*, 51−61.

(157) Chan, S. T.; Ermak, D. L.; Morris, L. K. *J. Hazard. Mater.* **1987**, *16*, 267−292.

(158) Sun, B.; Utikar, R. P.; Pareek, V. K.; Guo, K. *J. Loss Prev. Process Ind.* **2013**, *26*, 117−128.

(159) Riddle, A.; Carruthers, D.; Sharpe, A.; McHugh, C.; Stocker, J. *Atmos. Environ.* **2004**, *38*, 1029−1038.

(160) Rigas, F.; Sklavounos, S. *Chem. Eng. Sci.* **2006**, *61*, 1444−1452.

(161) Hanna, S. R.; Chang, J. C. *Atmos. Environ.* **2001**, *35*, 2231−2242.

(162) Luketa-Hanlin, A.; Koopman, R. P.; Ermak, D. L. *J. Hazard. Mater.* **2007**, *140*, 504−17.

(163) Qiao, Y.; West, H. H.; Mannan, M. S.; Johnson, D. W.; Cornwell, J. B. *J. Hazard. Mater.* **2006**, *130*, 155−162.

(164) Johnson, D. W.; Cornwell, J. B. *J. Hazard. Mater.* **2007**, *140*, 535−540.

(165) Fay, J. A. *J. Hazard. Mater.* **2003**, *96*, 2−3.

(166) Lehr, W.; Simecek-Beatty, D. *J. Hazard. Mater.* **2004**, *107*, 1−2.

(167) Vílchez, J. A.; Villafañe, D.; Casal, J. *J. Hazard. Mater.* **2013**, *246−247*, 181−188.

(168) Ponchaut, N. F.; Kytömaa, H. K.; Morrison, D. R.; Chernovsky, M. K. *J. Loss Prev. Process Ind.* **2011**, *24*, 870−878.

(169) Melton, T. A.; Cornwell, J. B. *J. Loss Prev. Process Ind.* **2010**, *23*, 762−767.

(170) Gavelli, F.; Chernovsky, M. K.; Bullister, E.; Kytomaa, H. K. *J. Hazard. Mater.* **2010**, *180*, 332−339.

(171) Giannissi, S. G.; Venetsanos, A. G.; Markatos, N.; Bartzis, J. G. *J. Loss Prev. Process Ind.* **2013**, *26*, 245−254.

(172) Würtz, J.; Bartzis, J.; Venetsanos, A.; Andronopoulos, S.; Statharas, J.; Nijsing, R. *J. Hazard. Mater.* **1996**, *46*, 273−284.

(173) Bartzis, J. G. *ADREA-HF: A Three-Dimensional Finite Volume Code for Vapour Cloud Dispersion in Complex Terrain*; Institute for Safety Technology, Joint Research Center, Commission of the European Communities: Brussels, Belgium, 1991.

(174) Venetsanos, A. G.; Papanikolaou, E.; Bartzis, J. G. *Int. J. Hydrogen Energy* **2010**, *35*, 3908−3918.

(175) Vesovic, V. *J. Hazard. Mater.* **2007**, *140*, 518−26.

(176) Siuta, D.; Markowski, A. S.; Mannan, M. S. *J. Loss Prev. Process Ind.* **2013**, *26*, 418−426.

(177) Britter, R. E.; McQuaid, J. *Workbook on the Dispersion of Dense Gases*; Health and Safety Executive: Liverpool, U.K., 1988.

(178) Ivings, M. J.; Lea, C. J.; Webber, D. M.; Jagger, S. F.; Coldrick, S. *J. Loss Prev. Process Ind.* **2013**, *26*, 153−163.

(179) Carissimo, B.; Jagger, S. F.; Daish, N. C.; Halford, A.; Selmer-Olsen, S.; Riikonen, K.; Perroux, J. M.; Wurtz, J.; Bartzis, J. G.; Duijm, N. J. *Int. J. Environ. Pollut.* **2001**, *16*, 614−629.

(180) Daish, N. C.; Britter, R. E.; Linden, P. F.; Jagger, S. F.; Carissimo, B. *Int. J. Environ. Pollut.* **2000**, *14*, 39−51.

(181) Duijm, N. J.; Carrissimo, B. *Evaluation Methodologies for Dense Gas Dispersion Models*; McGraw-Hill: New York, 2002.

(182) Ivings, M. J.; Jagger, S. F.; Lea, C. J.; Webber, D. M. *Evaluating Vapour Dispersion Models for Safety Analysis of LNG Facilities*; Fire Protection Research Foundation: Quincy, MA, 2007.

(183) Hansen, O. R.; Gavelli, F.; Ichard, M.; Davis, S. G. *J. Loss Prev. Process Ind.* **2010**, *23*, 857−877.

(184) Raj, P. P. K.; Moussa, A. N.; Aravamudan, K. *Experiments Involving Pool and Vapor Fires from Spills of Liquefied Natural Gas on Water*; Arthur D. Little, Inc.: Cambridge, MA, 1979; p 252.

(185) Schneider, A. L. US Coast Guard liquefied natural gas research at China Lake. *Proceedings of the Gastech 78 LNG−LPG Conference*; Monte Carlo, Monaco, Nov 7−10, 1978; pp 5−8.

(186) Raj, P. K.; Moussa, N. A.; Aravamudan, K.; Lind, C. D. *Oper. Sect. Proc.—Am. Gas Assoc.* **1979**, 246−251.

(187) Schneider, A. L. *J. Fire Flammability* **1980**, *11*, 302−313.

(188) Mizner, G. A.; Eyre, J. A. *EFCE Publ. Ser.* **1982**, *25*, 147−161.

(189) Hirst, W. J. S.; Eyre, J. A. Maplin Sands experiments 1980: Combustion of large LNG and refrigerated liquid propane spills on the sea. *Heavy Gas and Risk Assessment—II*; Springer: Dordrecht, Netherlands, 1983; pp 211−224.

(190) Rodean, H. C.; Hogan, W. J.; Urtiew, P. A.; Goldwire, H. C., Jr; McRae, T. G.; Morgan, D. L., Jr *Vapor Burn Analysis for the Coyote Series LNG Spill Experiments*; Lawrence Livermore National Laboratory (LLNL): Livermore, CA, 1984; p 89.

(191) Mizner, G. A.; Eyre, J. A. *Combust. Sci. Technol.* **1983**, *35*, 33−57.

(192) Nedelka, D.; Moorhouse, J.; Tucker, R. F. *The Montoir 35m Diameter LNG Pool Fire Experiments*; Midlands Research Station: Nice, France, 1989; p 16.

(193) Lowesmith, B. J.; Hankinson, G.; Acton, M. R.; Chamberlain, G. *Process Saf. Environ. Prot.* **2007**, *85*, 207−220.

(194) Studer, E.; Jamois, D.; Jallais, S.; Leroy, G.; Hebrard, J.; Blanchetière, V. *Int. J. Hydrogen Energy* **2009**, *34*, 9611−9619.

(195) Wu, Y.; Lu, Y.; Al-Rahbi, I. S.; Kalghatgi, G. T. *Int. J. Hydrogen Energy* **2009**, *34*, 5940−5945.

(196) Schneider, A. L. *J. Fire Flammability* **1980**, 302−313.

(197) Brown, L. E. *Hydrocarbon Process.* **1974**, 141−143.

(198) Raj, P.; Atallah, S. *Adv. Cryog. Eng.* **1975**, 143−150.

(199) Lautkasi, R. *J. Loss Prev. Process Ind.* **1992**, *5*, 175−180.

(200) Johnson, A. D. A model for predicting thermal radiation hazards from large-scale LNG pool fires. *Inst. Chem. Eng. Symp. Ser.* **1992**, 507−524.

(201) Moorhouse, J.; Pritchard, M. J. Thermal radiation hazards from large pool fires and fireballs—A literature review. *Inst. Chem. Eng. Symp. Ser.* **1982**, 397−428.

(202) Society of Fire Protection Engineers (SFPE). *The SFPE Handbook of Fire Protection Engineering*, 2nd ed.; SFPE: Bethesda, MD, 1995.

(203) Gavelli, F.; Davis, S. G.; Hansen, O. R. *J. Loss Prev. Process Ind.* **2011**, *24*, 908−915.

(204) Abe, A.; Katayama, M.; Kim, D.; Usuba, S.; Castillo, M.; Wakatsuki, M.; Kakudate, Y.; Tanaka, K.; Watanabe, Y. Numerical

prediction of blast effecs caused by large-scale exlosion of LOX/LNG fuel. *Proceedings of the International Symposium on Structures under Earthquake, Impact, and Blast Loading (IB'08)*; Osaka, Japan, Oct 10–11, 2008.

(205) Fay, J. A. *Annu. Rev. Energy* **1980**, *5*, 89–105.

(206) Raj, P. K. *J. Hazard. Mater.* **2008**, *157*, 247–259.

(207) Pérez, J. F. S.; Ferradás, E. G.; Alonso, F. D.; García, D. P.; Cano, M. V. M; Cotorruelo, J. Á. B. *Process Saf. Environ. Prot.* **2010**, *88*, 109–113.

(208) Alonso, F. D.; Ferradás, E. G.; Sánchez, T. d. J. J.; Aznar, A. M.; Gimeno, J. R.; Alonso, J. M. *J. Hazard. Mater.* **2008**, *150*, 146–152.

(209) Netherlands Organisation for Applied Scientific Research (TNO). *Methods for the Determination of Possible Damage*; TNO: The Hague, Netherlands, 1989.

(210) Pitblado, R. M.; Burns, D. J. *Chem. Eng. Prog.* **1989**, *85*, 69–75.

(211) Stoll, A. M.; Chianta, M. A. *Trans. N. Y. Acad. Sci.* **1971**, *33*, 649–670.

(212) Lihou, D.; Maund, J. Thermal radiation hazard from fireballs. *Inst. Chem. Eng. Symp. Ser.* **1982**, 191–224.

(213) Bernatik, A.; Senovsky, P.; Pitt, M. *J. Loss Prev. Process Ind.* **2011**, *24*, 19–24.

(214) U.S. Government. *National Infrastructure Protection Plan*; U.S. Department of Homeland Security: Washington, D.C., 2009.

(215) Yun, G.; Rogers, W. J.; Mannan, M. S. *J. Loss Prev. Process Ind.* **2009**, *22*, 91–96.

(216) Rathnayaka, S.; Khan, F.; Amyotte, P. *J. Loss Prev. Process Ind.* **2012**, *25*, 414–423.

(217) Parihar, A.; Vergara, C.; Clutter, J. K. *Saf. Sci.* **2011**, *49*, 686–694.

(218) Li, J.; Huang, Z. *Procedia Eng.* **2012**, *45*, 70–76.

(219) Pitblado, R. *J. Hazard. Mater.* **2007**, *140*, 527–534.

(220) Zhang, Q.-x.; Liang, D. *Procedia Eng.* **2013**, *52*, 602–606.

(221) Abbasi, T.; Abbasi, S. A. *J. Hazard. Mater.* **2007**, *141*, 489–519.

(222) Grossel, S. S. *J. Loss Prev. Process Ind.* **2008**, *21*, 492.

(223) Cheng, S.-R.; Lin, B.; Hsu, B.-M.; Shu, M.-H. *Expert Syst. Appl.* **2009**, *36*, 11918–11924.

(224) Keshavarz, G.; Thodi, P.; Khan, F. *J. Loss Prev. Process Ind.* **2012**, *25*, 159–165.

(225) Suardin, J. A.; Wang, Y.; Willson, M.; Mannan, M. S. *J. Hazard. Mater.* **2009**, *165*, 612–622.

(226) Suardin, J. A.; Qi, R.; Cormier, B. R.; Rana, M.; Zhang, Y.; Mannan, M. S. *J. Loss Prev. Process Ind.* **2011**, *24*, 63–75.

(227) Sun, B.; Guo, K. *J. Loss Prev. Process Ind.* **2013**, *26*, 1246–1256.

(228) Taylor, D. W. *J. Hazard. Mater.* **2007**, *142*, 776–785.

(229) Raj, P. K.; Lemoff, T. *J. Loss Prev. Process Ind.* **2009**, *22*, 820–829.

(230) Tanabe, M.; Miyake, A. *J. Loss Prev. Process Ind.* **2010**, *23*, 507–514.

(231) Tanabe, M.; Miyake, A. *J. Loss Prev. Process Ind.* **2012**, *25*, 809–819.

(232) Vanem, E.; Antão, P.; Østvik, I.; de Comas, F. D. C. *Reliab. Eng. Syst. Saf.* **2008**, *93*, 1328–1344.

(233) Vandebroek, L.; Berghmans, J. *Procedia Eng.* **2012**, *45*, 21–26.

(234) Moon, K.; Song, S.-R.; Ballesio, J.; Fitzgerald, G.; Knight, G. *J. Loss Prev. Process Ind.* **2009**, *22*, 908–914.

(235) Chang, D.; Rhee, T.; Nam, K.; Chang, K.; Lee, D.; Jeong, S. *Reliab. Eng. Syst. Saf.* **2008**, *93*, 1877–1885.

(236) International Maritime Organisation (IMO). *International Code for the Construction and Equipment of Ships Carrying Liquefied Gases in Bulk: IGC Code*; IMO: London, U.K., 1993.

(237) United States Government Printing Office (U.S. GPO). Minimum relief capacities for cargo tanks containing compressed or liquefied gas, U.S. Coast Guard. *Code of Federal Regulations (CFR)*; U.S. GPO: Washington, D.C., 2013.

(238) Havens, J.; Venart, J. *J. Hazard. Mater.* **2008**, *158*, 273–279.

(239) Bang, C. S.; Kim, J. G.; Lee, D. G. *J. Adhes. Sci. Technol.* **2012**, *26*, 969–986.

(240) Lee, J.-S.; Ryu, Y.-S.; Kim, N.-I.; Kim, B.-J.; Kim, Y.-K.; Kim, M.-H. *Trans. Nonferrous Met. Soc. China* **2009**, *19* (Supplement1), s271–s275.

(241) Kim, B. G.; Lee, D. G. *Compos. Struct.* **2008**, *86*, 27–36.

(242) Yu, Y. H.; Kim, B. G.; Lee, D. G. *Compos. Struct.* **2012**, *94*, 462–468.

(243) Yu, Y. H.; Kim, B. G.; Lee, D. G. *Compos. Struct.* **2013**, *95*, 547–556.

(244) Chul Kim, B.; Ho Yoon, S.; Gil Lee, D. *Ocean Eng.* **2011**, *38*, 592–608.

(245) Graczyk, M.; Moan, T. *J. Offshore Mech. Arct. Eng.* **2010**, *133*, 21103–21103.

(246) Pistani, F.; Thiagarajan, K. *Ocean Eng.* **2012**, *52*, 60–74.

(247) Mitra, S.; Wang, C. Z.; Reddy, J. N.; Khoo, B. C. *Ocean Eng.* **2012**, *39*, 1–13.

■ NOTE ADDED AFTER ASAP PUBLICATION

There were errors in values given in Table 3 of the version of this paper published May 16, 2014. The correct version published June 9, 2014.